FIRENWOOD

Improved fire design of engineered wood systems in buildings

Sub report D3.4
Test series 3

Editors/Authors:
Patrick Dumler
Norman Werther
Stefan Winter

Deliverable Number: D3.4
Date of delivery: 14/09/2022
Month of delivery: M42

Gefördert durch:
Bundesministerium für Ernährung und Landwirtschaft
aufgrund eines Beschlusses des Deutschen Bundestages

The FIRENWOOD project is supported under the umbrella of ERA-NET Cofund ForestValue by Germany (Federal Ministry of Food and Agriculture (BMEL); Agency for Renewable Resources (FNR) project number FKZ 2219NR120), Sweden (The Swedish Research Council for Environment, Agricultural Sciences and Spatial Planning (FORMAS); Swedish Energy Agency (SWEA); Swedish Governmental Agency for Innovation Systems (Vinnova) project number 2018-04989) and Norway (Research Council of Norway (RCN) project number 298587). ForestValue has received funding from the European Union's Horizon 2020 research and innovation programme under grant agreement No 773324.

Coordinator: Tian Li at RISE Fire Research AS

Table of Contents

Introduction

In test series 3 two different test setups were used. The aim of this series was to link the mechanical behavior of the joint with glued in rods to different temperatures. Therefore, test specimens with threaded rods were glued in parallel to grain direction in wooden specimens.

At first, reference tests at ambient temperature were carried out. Specimens were loaded mechanically under tension until failure. With these tests it was possible to derive the corresponding load levels for the tests with thermal load.

The second test setup included thermal tests. Here the specimens were loaded mechanically to a constant tensile load based on the reference tests. Meanwhile they were heated to a temperature of 110 °C. This test setup is intended to examine the critical adhesive temperature and the influence of various test configurations on the failure behavior.

The test series 3 can be divided into four parts. In test series 3.1, the reference tests took place under ambient temperature conditions. The creep tests with thermal loads were conducted within the test series 3.2 to 3.4. These differ in the level of mechanical load applied and in the execution of the joint of the test specimen.

1 Materials and Test Methods

1.1 Materials

Glued laminated timber made of spruce with the strength class GL 24h was used for all test specimens.

The test specimens were subjected to conditioning for at least 28 days at ambient temperature (20 °C, 65 % r. h.) until the equilibrium moisture content was reached. The density of the specimens was determined according to EN 408 on the entire test specimen. Drying samples were also taken from the test specimens in test series 3.2 to 3.4 in accordance with EN 13183-1. The density and moisture content were determined directly after the test took place and for comparison after the equilibrium moisture content had been reached. The mean moisture content was 12.5% before the tests were carried out.

The density of all test specimens according to EN 408 was 450 kg/m³ with a deviation of 5 %. A comparison of the densities of the specimen in test series 3.2 -3.4 taken from the entire test specimen and from the drying samples showed a difference of less than 2 %. The individual densities are listed in Appendix A and B.

Metric threaded rods of strength class 8.8 according to DIN 976 were used. The high strength class was chosen in order to be able to rule out a steel failure during test series 3.1. The nominal rod diameters used were 12 mm and 20 mm.

A two-component epoxy resin (Adhesive 1) and a two-component polyurethane (Adhesive 2) were used for gluing. The data for the processing of the adhesives are given in Appendix C.

1.2 Test setup

The cross-sections were either 60 mm × 60 mm or 100 mm × 100 mm depending on the rod diameter. The required minimum edge distances of 2.5 * d_{rod} according to EN 1995-1-1 were maintained. Two GLT-beams were used for the production of one specimen. They were connected with a glued in rod. To apply the tensile load, two additional rods were attached to each outer end of the specimen. The distance between the central rod and the outer rods l_m was at least 1.4 * the glued in length of the outer rod in accordance with EN 17334.

Two glue line thicknesses of 1 mm and 3 mm were investigated. With the glue line thickness of 3 mm, spacers made of plastic caps were installed at the rod ends so that the rod was centered in the borehole. The embedment length was therefore extended by the height of one spacer. The specimen design is shown in Figure 1.

Thermocouples Type K were positioned at the edge of the borehole at a distance of 50 mm from the joint and 20 mm from the end of the borehole.

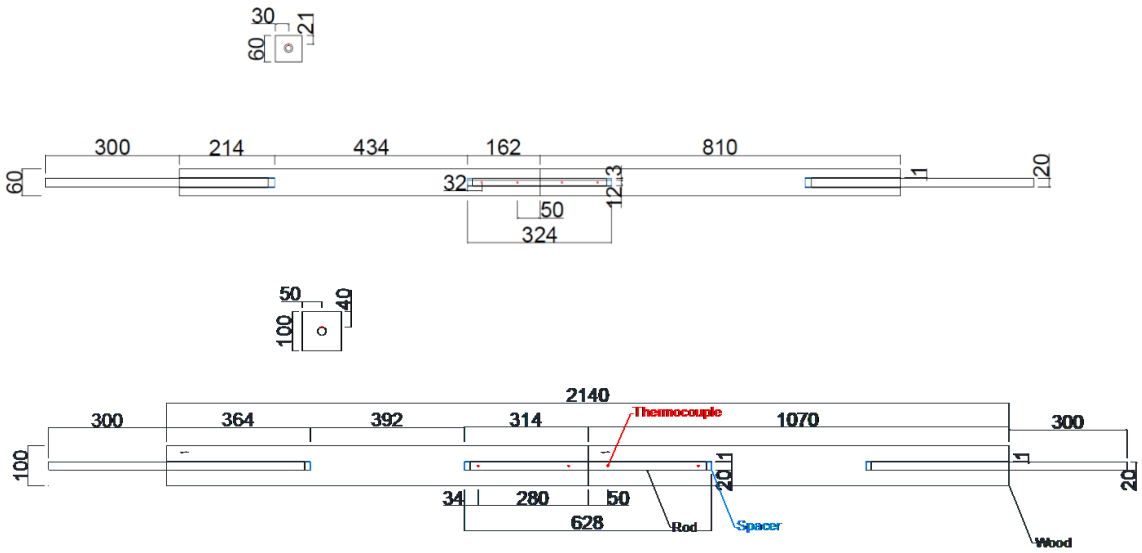

Figure 1: Sections and temperature measurement points of the specimens used in test series 3

Four testing setups were distinguished in test series 3:

- 3.1 Reference tests at ambient temperature
- 3.2 Creep tests under thermal load with 40 % of the reference load
- 3.3 Creep tests under thermal load with 60% of the reference load
- 3.4 Creep tests under thermal load with 40% of the reference load; Gap in the joint of 2 mm thickness

The specimens were named using five digits. The first digit stands for the test configuration. The second digit of the test specimen number designates the type of the adhesive. The third digit indicates the borehole diameter of the middle rod. The fourth digit shows the embedment length and the fifth digit shows the specimen number per configuration. The systematic structure of the test specimen number is shown in Table 1.

Table 1: Naming system of specimens

Spot	Meaning	Possible Number	Classification
1. Digit	Testing setup	1 / 2 / 3 / 4	Reference / 0,4 × Reference load / 0,6 × Reference load / 0,4 × Reference load and 2 mm joint gap
2. Digit	Adhesive type	1 / 2	Adhesive 1 / Adhesive 2
3. Digit	Borehole diameter	1 / 2 / 3 / 4	14 / 18 / 22 / 26 mm
4. Digit	Embedment length	1 / 2	150 resp. 162 / 300 resp. 314 mm
5. Digit	Configuration number	1 / 2	Identical construction Nr. 1 / 2

Table 2 shows a general overview of the design parameters of all test specimens in test series 3.

Table 2: Specimen configuration in test series 3 [1]

Specimen Number	Adhesive	Glue line thick-ness[mm]	Wood Cross section [mm × mm]	Specimen Length [mm]	Diameter rod [mm]	Embed-ment Length [mm]
11111	1	1	60 × 60	1620	12	162
11112	1	1	60 × 60	1620	12	162
11211	1	3	60 × 60	1620	12	162
11212	1	3	60 × 60	1620	12	162
12111	2	1	60 × 60	1620	12	162
12112	2	1	60 × 60	1620	12	162
12211	2	3	60 × 60	1620	12	162
12212	2	3	60 × 60	1620	12	162
11311	1	1	100 × 100	2140	20	150
12311	2	1	100 × 100	2140	20	150
11321	1	1	100 × 100	2140	20	300
11322	1	1	100 × 100	2140	20	300
11421	1	3	100 × 100	2140	20	314
11422	1	3	100 × 100	2140	20	314
12321	2	1	100 × 100	2140	20	300
12322	2	1	100 × 100	2140	20	300
12421	2	3	100 × 100	2140	20	314
12422	2	3	100 × 100	2140	20	314
21111	1	1	60 × 60	1620	12	162
21211	1	3	60 × 60	1620	12	162
22111	2	1	60 × 60	1620	12	162
22211	2	3	60 × 60	1620	12	162
21311	1	1	100 × 100	2140	20	150
22311	2	1	100 × 100	2140	20	150
21321	1	1	100 × 100	2140	20	300
21421	1	3	100 × 100	2140	20	314
22321	2	1	100 × 100	2140	20	300
22421	2	3	100 × 100	2140	20	314
31111	1	1	60 × 60	1620	12	162
32111	2	1	60 × 60	1620	12	162
31321	1	1	100 × 100	2140	20	300
32321	2	1	100 × 100	2140	20	300
41111	1	1	60 × 60	1620	12	162
42111	2	1	60 × 60	1620	12	162

1.3 Manufacturing

The test specimens were each composed of two halves. For this purpose, the glulam beams were sawn to the lengths planned for each test specimens.

At first boreholes corresponding to the length of the rod were drilled into the glulam beams using an auger bit and a drill stand. The boreholes had a diameter between 14 and 26 mm. The embedment length for each specimen half was 150 mm for the rod diameter of 12 mm

and 300 mm for the rod diameter of 20 mm. The spacers used to center the rods with glue line thicknesses of 3 mm didn`t have a load bearing function (see Figure 2). Therefore, the borehole depth was increased by the height of one spacer with 12 mm for the smaller rod diameter and 14 mm for the rod diameter of 20 mm. The effective anchorage length was therefore not changed. The borehole depth for the M12 rods with a glue line thickness of 1 mm had a wrong length of 162 mm. The longer embedment length was considered accordingly in the calculations.

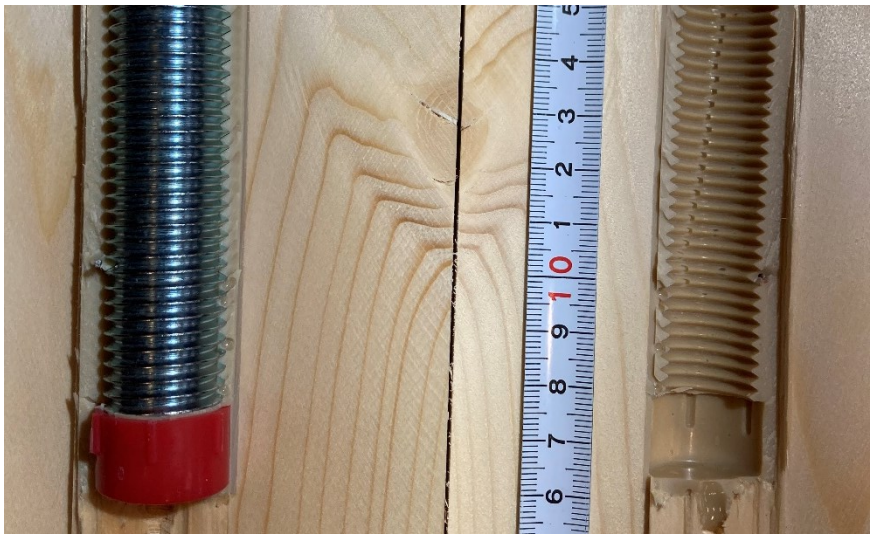

Figure 2: Spacer for the centering of the rod with a glue line thickness of 3 mm

To fill in the adhesive, an opening with a diameter of 8 mm was drilled at a distance of 1 cm from each borehole end. The boreholes were then cleaned with compressed air.

The rods were inserted into the two test specimen halves. They were cleaned with compressed air and purifiers. In the case of test specimens with a glue line thickness of 3 mm, spacers were placed on the thread at the end of the rod, which ensured central positioning in the drill hole and were intended to ensure an even thickness of the adhesive layer. In this way, eccentricities that reduce the load-bearing capacity can be reduced to a minimum. The two halves of the test specimen were compressed and the joint area was sealed with an adhesive tape to prevent the adhesive from leaking.

Holes with a diameter of 2 mm were then drilled into the side of each specimen to insert thermocouples type K for temperature measurement. At first a drill press was used for pre-drilling. The drilled tips of the type K thermocouples were cut to a length of 5 mm each. The drill hole depth was therefore 35 mm for the cross section of 60 mm x 60 mm and 55 mm for the cross section of 100 mm x 100 mm. It should be noted that the thermocouples do not run along the isotherms in the test specimen due to the installation process. Due to the tensile load applied in the tests, this method was not used in order to not weaken the glue line and the cross-section. This measurement method did not require to halve the specimens along the longitudinal axis to insert the thermocouple and glue them together afterwards like in test series 2.1.

The two-component adhesives were pressed into one opening using a static mixer attachment so that the manufacturer's recommended mixing ratio between resin and hardener was achieved. The other hole on the second half of the specimen was used as a vent hole. The cartridges were not changed during the gluing process in order to avoid air bubbles in the glue line. The adhesive was pressed inside the hole until a leakage was seen from the ventilation opening. Both openings were then closed with wooden dowels.

After a drying time of at least 7 days, the first rods on the specimen ends were glued. For this purpose, the test specimens were set up vertically. The borehole was used as a ventilation

opening. An inlet opening is bored at a distance of 1 cm above the end of the borehole. After the curing phase this procedure was repeated on the other side (see Figure 3).

In test series 3.4 a gap of 2 mm was set between two specimen halves. Therefore, the rod had a length of 326 mm. The gap was manufactured with the aid of a flat washer as a spacer between the wooden halves.

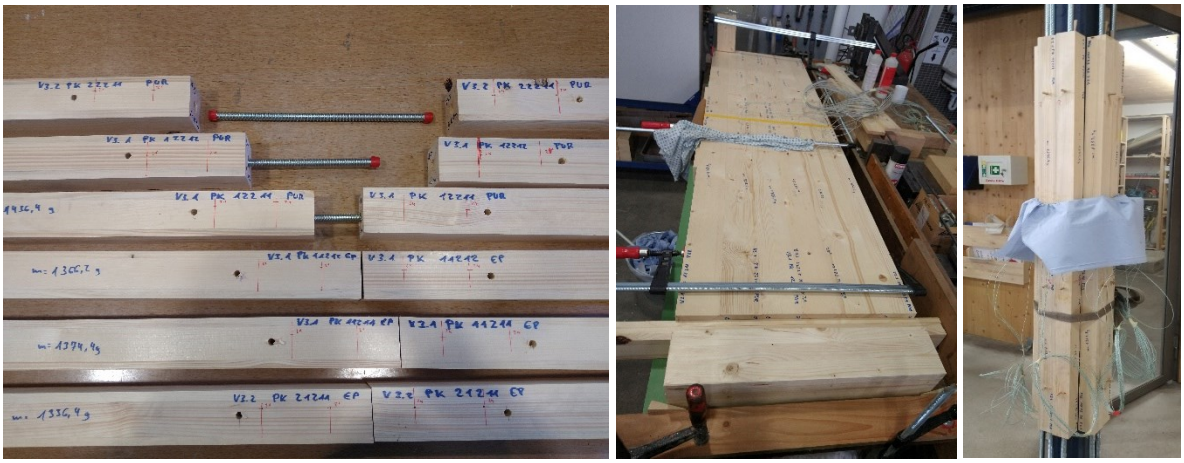

Figure 3: Manufacturing process of specimens

1.4 Testing equipment

1.4.1 Load application

To apply the load, a hollow-piston cylinder was used which was operated via compressed air. Due to the reduction in pressure during the test, it had to be recalibrated. A rod was passed through the hollow piston cylinder and secured by a nut and a lock nut. As soon as compressed air was applied, the hydraulic cylinder pressed against a steel support in a steel frame, applying tensile load to the secured rod. The test specimen was connected to this rod with a long nut. On the other side, the specimen was clamped to the steel frame. The sensor 26K - 500kN (E 96060) was used to measure the load (see Figure 4).

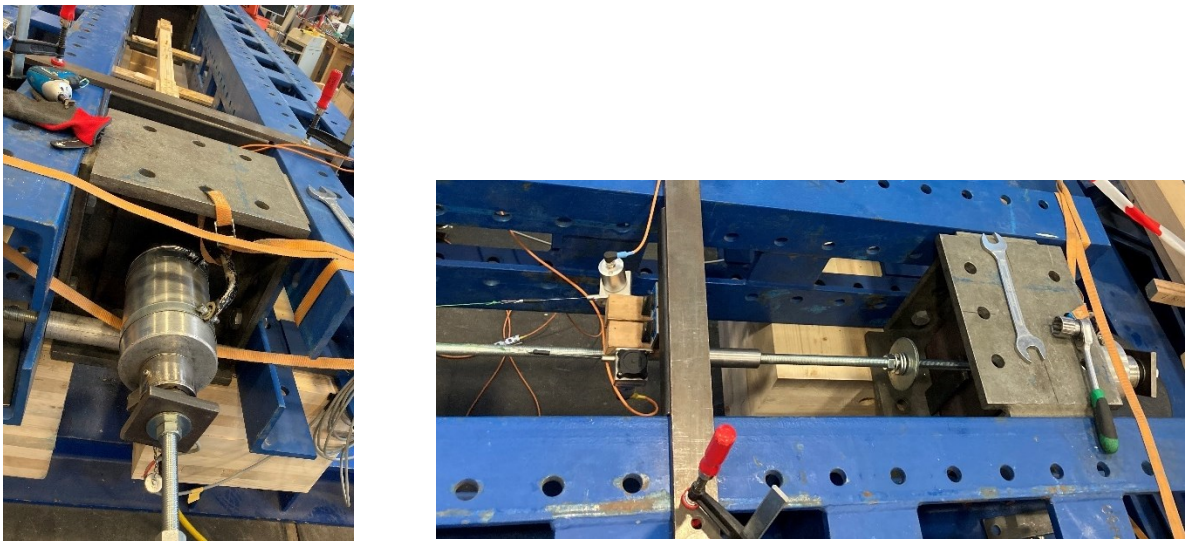

Figure 4: Load application (left) and connection to specimen (right) in the steel frame

The deformation of the specimen was measured using two WayCon SX50 draw-wire sensors. The two ends of the wire were each fastened on one side of the joint using eyebolts. The distances were chosen to be the same for all specimens. The distance to the joint was 3 cm on both halves and between each eyebolt 2 cm (see Figure 5).

In this way two deformations for each specimen half were measured. The difference between them gives the net displacement of the entire test specimen. A measurement of the individual rods was not possible due to the testing setup. Before each test, it was checked that the wires could swing freely and without resistance.

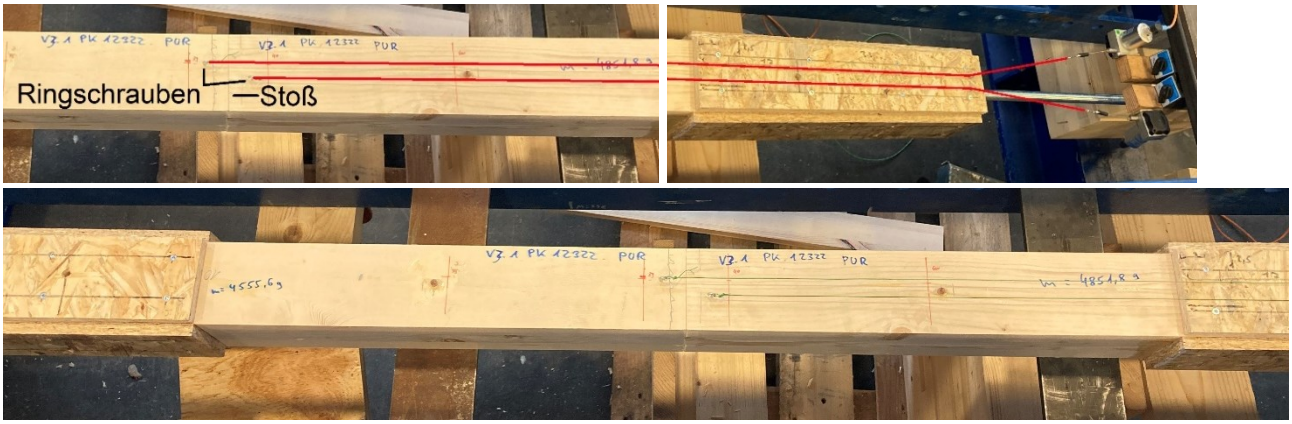

Figure 5: Deformation measurement of specimen [1]

1.4.2 Thermal box

A thermal box was used to create an air temperature of 110 °C for the test series 3.2 – 3.4 (creep tests under thermal load). The box was positioned between the steel frame and covered the middle part of the specimens. All walls of the box were insulated with mineral wool panels to reduce the heat loss during testing. Additional panels for the inside of the box were used. These were covered with aluminum foil and had a thickness of 3 cm. The openings and joints of the box were sealed with airtight tape (see Figure 6).

The side openings for inserting the specimens were about 14 cm wide and 14 cm high. In order to keep the thermal bridges in this area as low as possible, the gaps were filled with mineral wool and protected by additional insulation boards from the outside.

The box had two additional openings on the bottom side. One was used as an inlet for the heated air supply. The other one was used as an outlet.

Figure 6: Testing setup for creep tests under thermal load

1.4.3 Thermal input

The test specimens were heated mainly by convection. The air was blown into the thermal box using a medium-pressure fan type MD10 from Herz. An electric heater was placed between the fan and the box to heat the supplied air. The heated air was led back into the blower via the outlet in the thermal box, creating a closed circuit (see Figure 7).

The measuring device E.T.R. 4824 of the brand Herz was used to control the temperature. The frequency of the fan could be adjusted with the low-voltage converter Commander C200 from Control Techniques. A high frequency of around 46 Hz was chosen so that there were no significant fluctuations. At a maximum possible frequency of 50 Hz, the fan produces an air flow of 4.9 m^3/min.

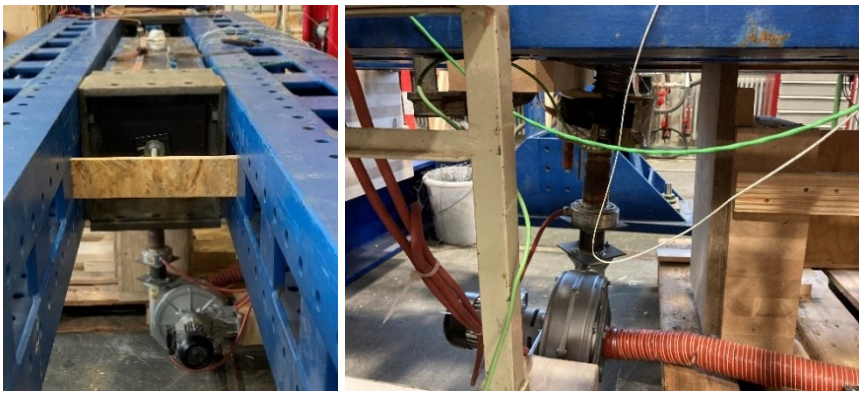

Figure 7: Connection of the fan to the thermal box [1]

1.4.4 Temperature measurement

The air temperature the oven as well as in the specimens was measured with the help of thermocouples type K. They were connected to the multi-channel data logger midiLogger GL840 from Graphtec.

In one specimen four thermocouples were inserted. They were named after the channel used in the data logger (CH1 - CH4). The positions are shown in Figure 8.

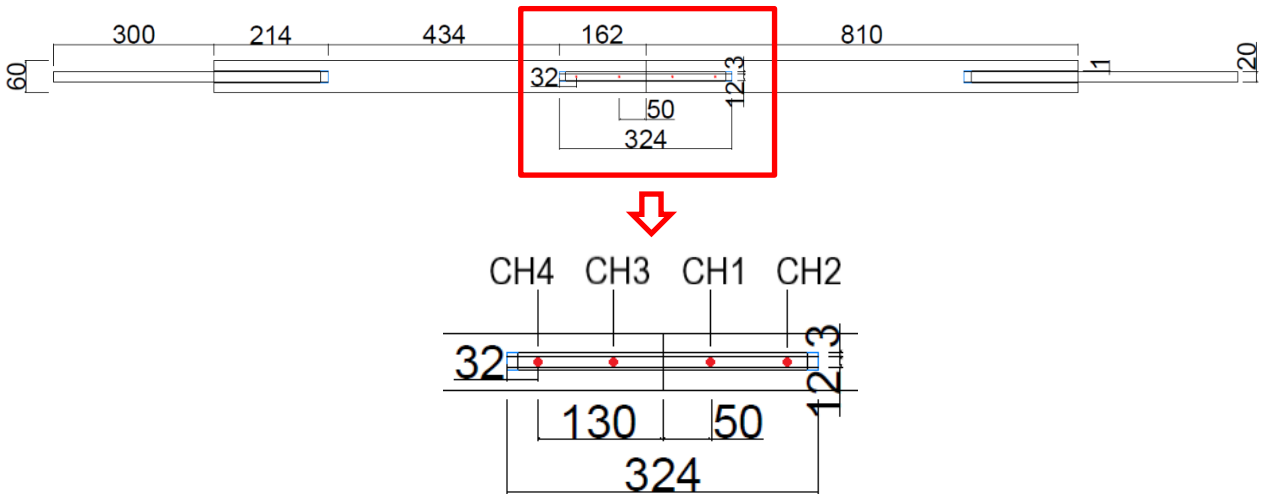

Figure 8: Positions of the thermocouples CH1 – CH4

For measurement of the air temperature also four thermocouples were used (CH17 - CH20). At first only two measurement points were installed in the direct vicinity of the joint in the middle of a specimen (CH19 & CH20). Due to the heating setup a temperature gradient from the inlet to the outlet was present. Therefore, additional measuring points were subsequently attached in the area of the inlet and outlet during the tests (CH17 & CH18). Their position can be seen in Figure 9.

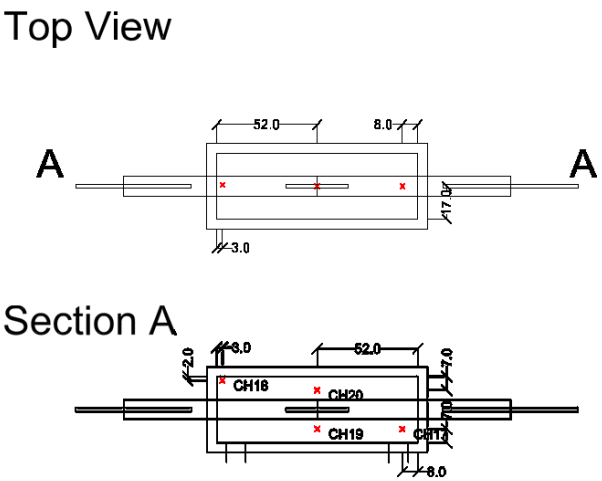

Figure 9: Positions of the thermocouples CH17 – CH20 for the measurement of the air temperature inside the thermo box

1.5 Test procedure

The test specimens from test series 3.1 (reference tests at ambient temperature) were loaded with an increasing tensile force until failure of the specimen. For each configuration two identical designed specimens were tested. The mean values of the failure load of both specimens were used as a reference load for the creep tests under thermal load.

In the test series 3.2 – 3.4 (creep tests under thermal load) a constant mechanical tensile load was applied on the specimens based on the results from the reference tests. At the same time, the temperature in the oven was heated up to 110 °C. At the beginning of the experiment, ambient temperature conditions prevailed. Due to bigger deformations with higher temperatures the mechanical load had to be readjusted during the test. The decrease in the load and the adjustments made can be seen in the deformation diagrams in Appendix G. The deviation of the load level to the target value was kept in an area of approx. -0,5 and +0,5 kN.

The mechanical load management for the different test configurations can be seen in Figure 10. The load applied is shown on the vertical axis and the time on the horizontal axis. The left diagram shows the typical load curve for the reference tests whereas on the right diagram the constant load level for the creep tests with thermal load is shown.

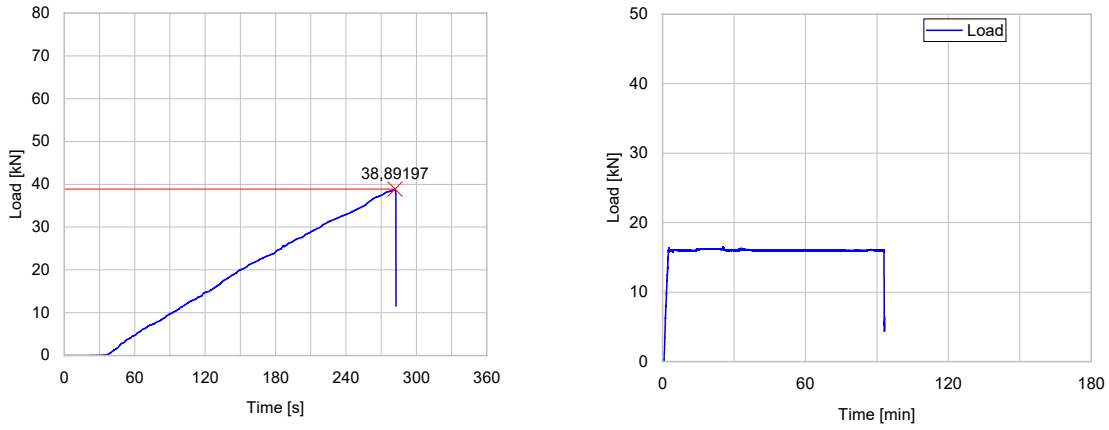

Figure 10: Load management for reference tests (left) and creep tests (right) [1]

The specimens of test series 3.1 didn`t have reinforcement measures against lateral failure of the wood. Therefore, the specimens 11322 and 11421 did not fail at the central connection as planned, but near the support. The two measured values for the failure load were nevertheless considered in the evaluation because they showed significantly higher failure loads than their respective identical twins in this testing configuration. Also, since the failure appeared at the outer joint of the specimen it is assumed that the central connection would have carried even higher loads. In order to prevent the wood from splitting at the ends of the specimen as a result of transverse tensile stresses, oriented stranded boards were attached on all four sides as a reinforcement measure in the further tests. Afterwards all specimens showed a failure as planned in the middle connection.

During the tests, the temperature at the edge of the borehole, the air temperature, the load level and the deformation were recorded.

Table 3 shows the failure loads of the reference tests and the resulting loads of the creep tests under thermal load.

In order to assess the load-bearing capacity of components and connections in the event of fire, it is necessary to define the load-bearing capacity level required by calculation. This is always significantly below the load-carrying capacity at ambient temperature, since it is an exceptional situation design case and reduced safety factors may be applied (DIN EN 1990).

The required load-bearing capacity can be determined by comparing the design models in DIN EN 1995-1-1 (design at normal temperature) and DIN EN 1995-1-2 (design in case of fire). [2, 3] If the load-bearing capacity of a timber construction connection under normal temperature by calculation is 100% utilized, its design load-bearing capacity in the event of fire must reach 28% - 51% of the characteristic value under normal temperature in order to be able to fulfill the of load-bearing capacity in the event of fire. This relationship results from the following consideration:

Dimensioning of the load-bearing capacity under normal temperature according to DIN EN 1995-1-1:

$$E_d \leq k_{mod} \cdot \frac{R_k}{\gamma_M} = (0{,}6 \ldots 1{,}1) \cdot \frac{R_k}{1{,}3} = (0{,}46 \ldots 0{,}85) \cdot R_k \quad (1)$$

With:

- E_d Design value of stresses at normal temperature for the basic combination of actions, see DIN EN 1990 [4]
- R_k Characteristic resistance of the connection in kN
- k_{mod} Modification factor for load duration and moisture content (varies in the range between 0.6 and 1.1 depending on length of load duration and service class)
- γ_M Partial safety factor for a building material, taking model uncertainties and geometric deviations into account

Design of the load-bearing capacity in case of fire according to DIN EN 1995-1-2:

$$E_{d,fi} = \eta_{fi} \cdot E_d = 0{,}6 \cdot E_d \leq k_{mod,fi} \cdot \frac{k_{fi} \cdot R_k}{\gamma_{M,fi}} = 1{,}0 \cdot \frac{1{,}05 \cdot R_k}{1{,}0} \approx 1{,}0 \cdot F_{V,k} \quad (2)$$

With:

- $E_{d,fi}$ Design value of stresses on the connection/component in the event of fire
- $k_{mod,fi}$ Modification factor for load duration and moisture content in case of fire 1.0
- $\gamma_{M,fi}$ Partial safety factor for a building material in case of fire 1.0
- k_{fi} Coefficient for determining the 20 % - fractile value (here related to fasteners)
- η_{fi} Reduction factor for the design value in the event of a fire (usual 0.6 in timber construction for residential and office use)

Substituting equation (1) into (2):

$$E_{d,fi} = E_{k,fi} = 0{,}6 \cdot (0{,}46 \ldots 0{,}85) \cdot R_k = (0{,}28 \ldots 0{,}51) \cdot R_k \quad (3)$$

The range between 28 % and 51 % results from the different values to be applied for k_{mod} in the design at ambient temperature. In addition, variations can result from the type of use and thus the relationship between permanent load and live load.

Assuming k_{mod} = 0.8 and using the component in a residential building, the required load level is around 37 % between the characteristic load-bearing capacities in the event of fire and at normal temperature. A component that is fully loaded must therefore reach at least this load level in the event of fire in order to fulfill both verifications. In cases where certain components do not achieve the required load-bearing capacity level in the event of fire, the verification in the cold state cannot be fully utilized. [5]

At least three test specimens are required to determine the characteristic load-bearing capacity according to EN 14358. [6] Since only two test specimens per configuration were available in the reference tests, the characteristic value could not be determined.

For this reason, two different load levels were applied with 40 % and 60 % of the mean failure loads of the reference specimens. The value of the calculated characteristic load-carrying capacity according to EN 1995-1-1 is significantly lower than the loads to be applied in the tests (see Table 3).

Table 3: Failure loads and load levels for creep tests under thermal load based on reference test and design model

Specimen Number	Wood Cross section [mm × mm]	Failure load / Planned load [kN]		Char. Design load EN 1995-1-1
11111	60 × 60	F_{max}	38,69	29,31
11112	60 × 60	F_{max}	46,61	29,31
11211	60 × 60	F_{max}	41,80	27,14
11212	60 × 60	F_{max}	45,86	27,14
12111	60 × 60	F_{max}	38,89	29,31
12112	60 × 60	F_{max}	41,24	29,31
12211	60 × 60	F_{max}	41,36	27,14
12212	60 × 60	F_{max}	42,10	27,14
11311	100 × 100	F_{max}	66,32	45,24
12311	100 × 100	F_{max}	61,41	45,24
11321	100 × 100	F_{max}	89,62	84,82
11322	100 × 100	F_{max}	105,82	84,82
11421	100 × 100	F_{max}	131,51	84,82
11422	100 × 100	F_{max}	116,39	84,82
12321	100 × 100	F_{max}	100,82	84,82
12322	100 × 100	F_{max}	97,58	84,82
12421	100 × 100	F_{max}	121,56	84,82
12422	100 × 100	F_{max}	110,87	84,82
21111	60 × 60	0,4 × F_{mean}/0,4 x F_{char}	17,06	11,72
21211	60 × 60	0,4 × F_{mean}/0,4 x F_{char}	17,53	11,72
22111	60 × 60	0,4 × F_{mean}/0,4 x F_{char}	16,03	10,86
22211	60 × 60	0,4 × F_{mean}/0,4 x F_{char}	16,69	10,86
21311	100 × 100	0,4 × F_{mean}/0,4 x F_{char}	26,53	18,1
22311	100 × 100	0,4 × F_{mean}/0,4 x F_{char}	24,56	18,1
21321	100 × 100	0,4 × F_{mean}/0,4 x F_{char}	42,33	33,93
21421	100 × 100	0,4 × F_{mean}/0,4 x F_{char}	49,58	33,93
22321	100 × 100	0,4 × F_{mean}/0,4 x F_{char}	39,68	33,93
22421	100 × 100	0,4 × F_{mean}/0,4 x F_{char}	46,89	33,93
31111	60 × 60	0,6 × F_{mean}/0,6 x F_{char}	25,59	11,72
32111	60 × 60	0,6 × F_{mean}/0,6 x F_{char}	24,04	11,72
31321	100 × 100	0,6 × F_{mean}/0,6 x F_{char}	63,49	33,93
32321	100 × 100	0,6 × F_{mean}/0,6 x F_{char}	59,52	33,93
41111	60 × 60	0,4 × F_{mean}/0,4 x F_{char}	17,06	11,72
42111	60 × 60	0,4 × F_{mean}/0,4 x F_{char}	16,03	11,72

After the failure in the test series 3.2 – 3.4 wooden slices were cut directly from the test specimens from an undamaged section without knots or other errors. These slices were weighed in order to determine the loss of moisture during the tests.

The test specimens had an average wood moisture content of 12.6 % at the start of the test. After the thermal loaded tests, the wood dried to an average density of 9.2 % (see Appendix B).

After the tests were completed, the test specimens were split lengthways in the area of the middle connection to better determine the mode of failure and the condition of the adhesive inside the borehole. The pictures of the split specimens are given in Appendix D.

2 Test results

2.1 Failure modes

The test specimens can fail in the three materials used. A distinction was made between the following failure modes.

- Adhesive failure
  - Adhesive failure adhesive – wood (a)
  - Adhesive failure adhesive – steel (b)
  - Cohesive failure (c)
- Wood failure
  - Shear fracture near the bond line (d)
  - Splitting of wood (e)
  - Tearing out with part of the surrounding wood (f)
  - Tensile fracture in wood (g) (did not occur)
- Steel failure by exceeding the yield point or the tensile strength (h) (did not occur)

Common failure modes are shown in Figure 11.

Adhesive failure adhesive-steel (b)	Mixed failure Adhesion adhesive-wood and adhesive-steel (a-b)	Shear fracture near the bondline (d)	Tearing out with part of the surrounding wood (f)
22211	31321	11321	12311

Figure 11: Common failure modes in test series 3

In most cases, a mixed failure could be identified. The wood often splits (e) during the creep tests. When analyzing the recordings, however, it became apparent that in some test specimens the splitting only occurred after the actual failure. This was only triggered when the test specimen was dismantled and the rod was pulled out completely. In the case of test specimens 22421 and 31111, it was no longer possible to determine when this splitting occurred. Therefore, the splitting of the wood was included in Figure 12.

Figure 12 shows the different failure modes for the reference tests and for the creep tests with thermal load. The adhesive failure shows a bluish discoloration while the wood failure is in the orange color range. It can be clearly seen that in the reference tests mainly failures in the wood occurred. Here a large part is due to a mixed fracture between splitting and tearing out with parts of the surrounding wood.

In comparison, the tests under thermal load clearly show that the adhesive becomes decisive in the event of failure. Only a small proportion of just about over 20% is associated with failure in the wood. Splitting was found for five specimens in test series 3.2 – 3.4. However, in the case of two of them it is unclear whether the splitting occurred during the test or only when the test specimen was removed from the steel frame.

An influence of the cross-section and the adhesive on the type of failure cannot be clearly determined. The corresponding diagrams for the different variants can be found in Appendix E.

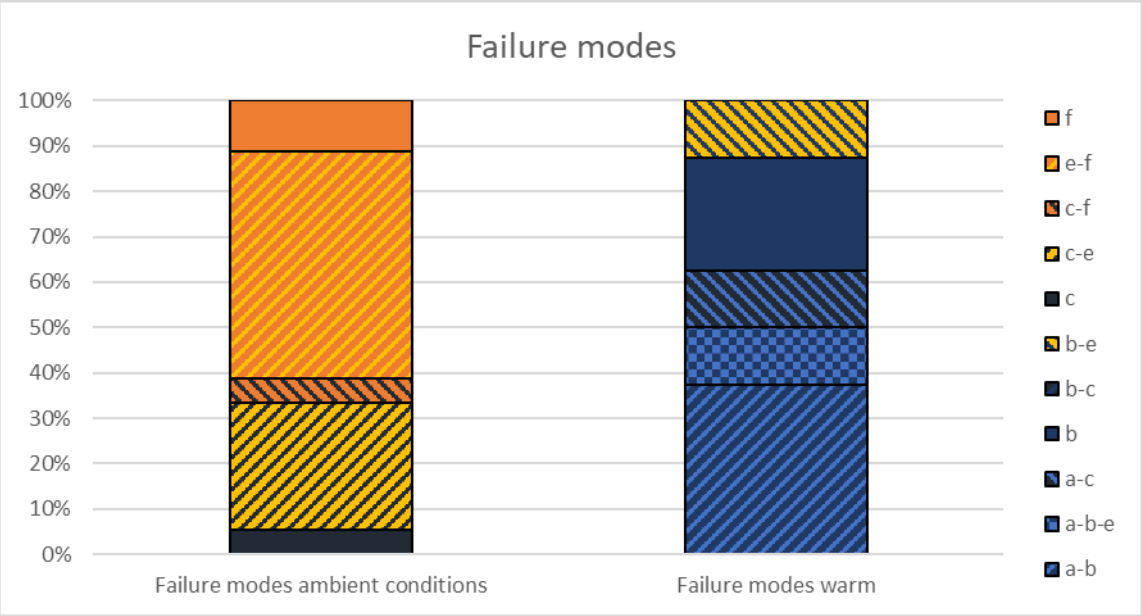

Figure 12: Overview of failure modes for test series 3 (Failure modes: Adhesive failure adhesive-wood (a), Adhesive failure adhesive-steel (b), Cohesive failure (c), Shear fracture near the bond line (d), Splitting of wood (e), Tearing out with part of the surrounding wood (f))

The results from the examination of the failed test specimens are shown in Table 4.

Table 4: Detailed failure modes for test series 3 [1]

Specimen Number	Adhesive failure adhesive – wood (a)	Adhesive failure adhesive – steel (b)	Cohesive failure (c)	Shear fracture near the bond line (d)	Splitting of wood (e)	Tearing out (f)
11111					×	×
11112					×	×
11211				×	×	

11212							×
12111						×	×
12112					×		×
12211						×	×
12212						×	×
11311						×	×
12311						×	×
11321					×	×	
11322					×	×	
11421						×	×
11422					×	×	
12321							×
12322					×	×	
12421						×	×
12422					×	×	
21111			×				
21211	×		×				
22111	×		×				
22211			×				
21311			×			×	
22311	×				×		
21321	×		×				
21421	×		×				
22321	×		×				
22421			×			×	
31111	×		×			×	
32111	×				×		
31321	×		×				
32321			×				
41111			×			×	
42111	×		×			×	

2.2 Reference tests

2.2.1 Failure Load

For the specimens with a cross-section of 60 mm x 60 mm in test series 3.1, the failure load is shown in Figure 13. A distinction is made between the two adhesives and the glue line thickness. The square symbols show the results for a glue line thickness of 3 mm. It can be seen that the failure load for both adhesives is in the range of 45 kN. On average, the values for Adhesive 1 are slightly higher than for Adhesive 2. The thickness of the glue line did not result in any significant increase in the load-bearing capacity of the connection. Since the failure in both tests was mainly associated with splitting and tearing out of the wood, it is assumed that higher loads would have been achieved if a larger cross-section was selected, since the wood is the main cause of failure. For this reason, the values are in a similar range.

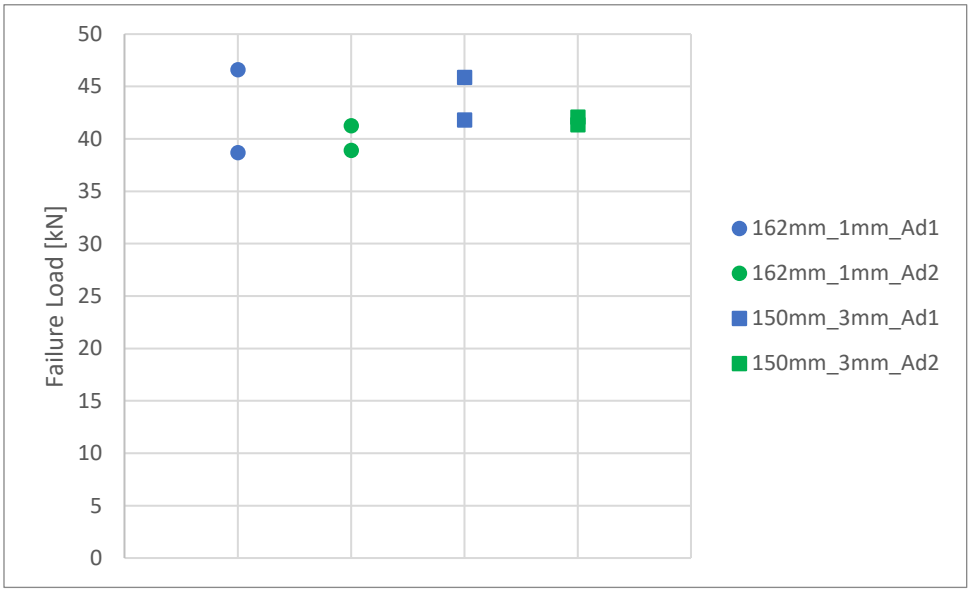

Figure 13: Failure load for specimens with cross-section of 60 mm x 60 mm for test series 3.1

The test specimens with a cross-section of 100 x 100 mm show significantly larger differences in their failure loads (see Figure 14). Due to the larger rod diameter with the embedment length of 150 mm, the test specimen for both adhesives failed approx. 20 kN later in the range of 60 - 65 kN. Due to the bigger rod and therefore bigger diameter of the borehole a larger adhesive surface for the transfer of shear stresses is present which can be the cause for the higher failure loads in comparison with the smaller rod diameters.

For a larger embedment length of the rod the failure loads rise. However, the increase is not proportional to the embedment length.

Increasing the glue line thickness further increases the failure load. Two reasons can be cause for the increase. The borehole again has a larger diameter, which creates a larger adhesion surface to the wood. Secondly, the lower stiffness of the adhesive is believed to reduce the stress peaks at the borehole ends, which are the cause for the splitting of the wood. Adhesive 1 showed a mean load-bearing capacity that was approx. 15% higher in the tests.

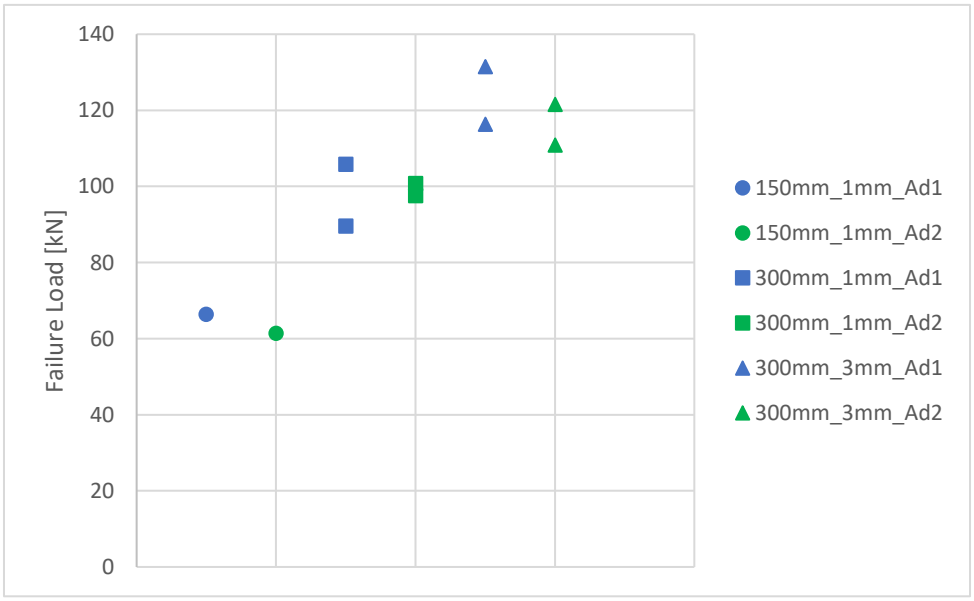

Figure 14: Failure load for specimens with cross-section of 100 mm x 100 mm for test series 3.1

2.2.2 Comparison of test results with design models

Figure 15 shows a comparison of the test results with the load-bearing capacity to be assumed by the design model of the draft of EN 1995-1-2. The values of the design model are on the y-axis. The test results for each specimen are shown on the x-axis. If the values are below the line of angle, the test results are therefore higher. In this case the design model predicts lower load-bearing capacities and shows more conservative results. If the values are higher, the connection is overestimated by the design model.

Three different embedment lengths can be recognized in the diagram. The lowest values are for the test with a cross section of 60 mm x 60 mm and a rod diameter of 12 mm. The highest results show the test results for M20 rods with an embedment length of 300 mm. The two results lying between them represent the M20 rods with a shorter embedment length of 150 mm.

The design model always proposes lower load-bearing capacities than in the tests. It also can be seen that for the M12 rods there are almost no differences depending on the adhesive type or the glue line thickness.

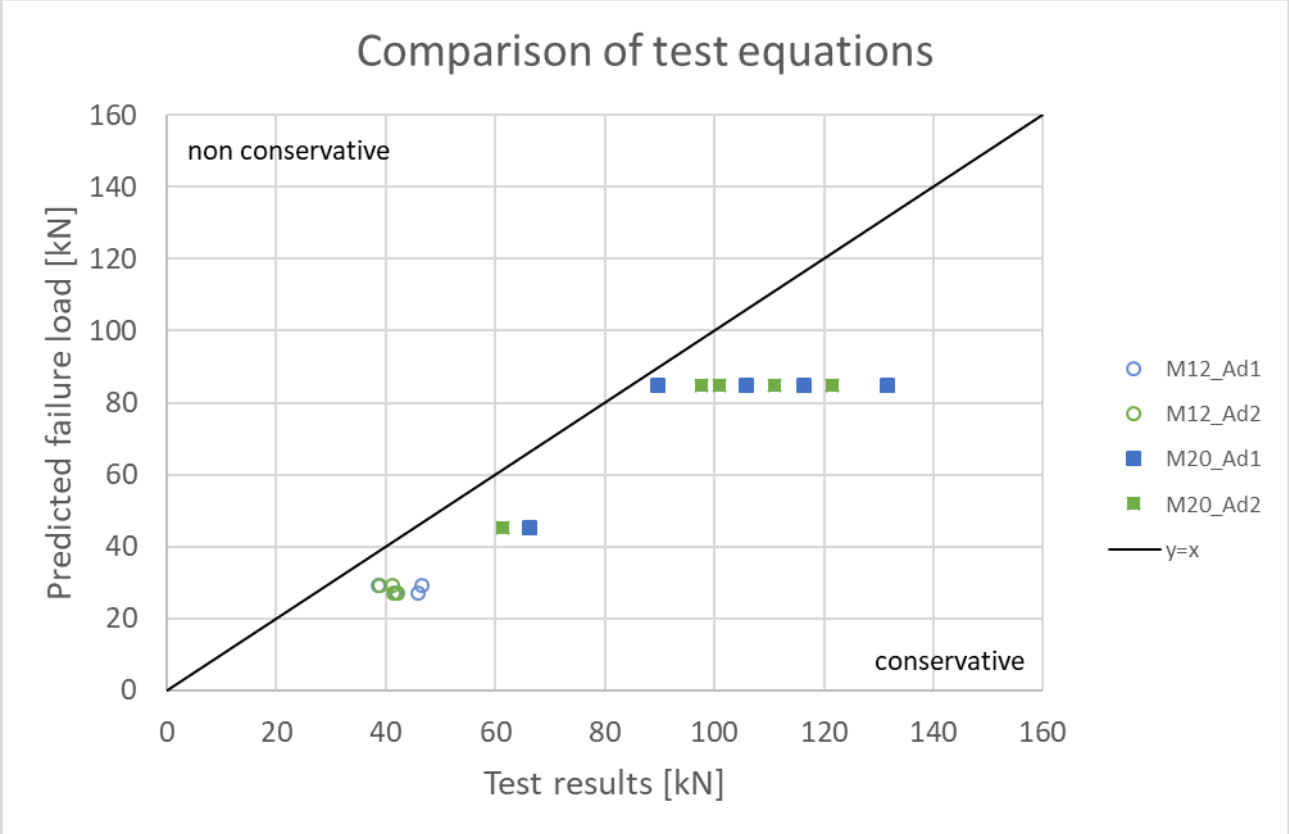

Figure 15: Comparison of test results with design model (blue: Adhesive 1, green: Adhesive 2)

2.3 Creep tests with temperature load

2.3.1 Failure temperatures

The test specimens failed as soon as the mechanical load could no longer be maintained despite readjustments. The temperature prevailing at the edge of the borehole at this time was defined as the failure temperature.

During the creep tests, it was seen that the temperature development in the thermo box was not uniform over the entire length of the box. The reason for this is the distribution of the supply and exhaust air openings, which caused a temperature gradient to form in the box. This can also be seen in the temperature measurements in the test specimens. CH3 and CH4 are closer to the inlet opening, which is why the higher temperatures are measured here in the event of failure than in CH1 and CH2 (see also Figure 9 for the position of the measuring points). Failure therefore always occurred in the half of the test specimen with the respective Channels CH3 and CH4. For this reason, the failure temperature was derived only from these two channels. Figure 16 shows the failure temperature for all channels of test series 3.2. In these, an increase in temperature can always be observed at the measuring points 3 and 4, regardless of the glue line thickness or the rod diameter.

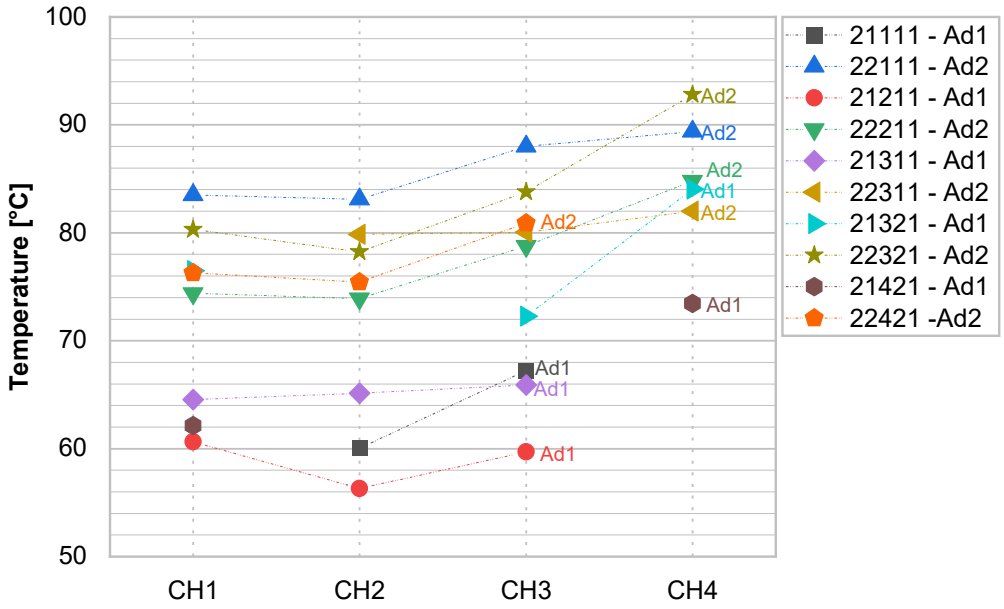

Figure 16: Failure temperatures of test series 3.2

Figure 17 shows the failure temperatures of the specimens in test series 1 (small scale tension shear tests) and 3 (creep tests with glued in rods) for Adhesive 1 with a load level of 40 % of the reference specimens. For test series 1 the different glue line thicknesses are compared with each other as well as the configuration with an air temperature of 130 °C. For test series 3 the two different cross-sections are compared.

Adhesive 1 reached failure temperatures in the range of approx. 65 °C to approx. 80 °C for test series 3. These were significantly higher than the temperatures from the tests in test series 1 with small-scale test specimens. It is assumed that the lower relative load is the reason. In test series 3 the load was related to the mean value and not to the maximum value like in test series 1. In test series 1, it was already determined that a higher load leads to earlier failure because the adhesive loses its strength with rising temperatures. When higher loads are applied the load-bearing capacity is exceeded faster which reduces the failure temperature.

In addition, it can be seen that the scattering of the results in the tests with glued in rods is higher. Since larger test specimens were used here, the probability of inhomogeneities in the wood as well as in the glue line increases. A more uniform heating of the glue line is more likely in the small-scale specimens since fewer influencing factors are present (inhomogeneities in the material area, area of the surface, temperature distribution, etc.). In addition, there

is more bound water in the test specimens of test series 3, which can also have a greater influence on the heating behavior of the glue line.

Higher failure temperatures were measured for the test specimens with a cross section of 100 mm x 100 mm than for the cross sections of 60 mm x 60 mm. No direct correlation could be found here with the other tests and the types of failure.

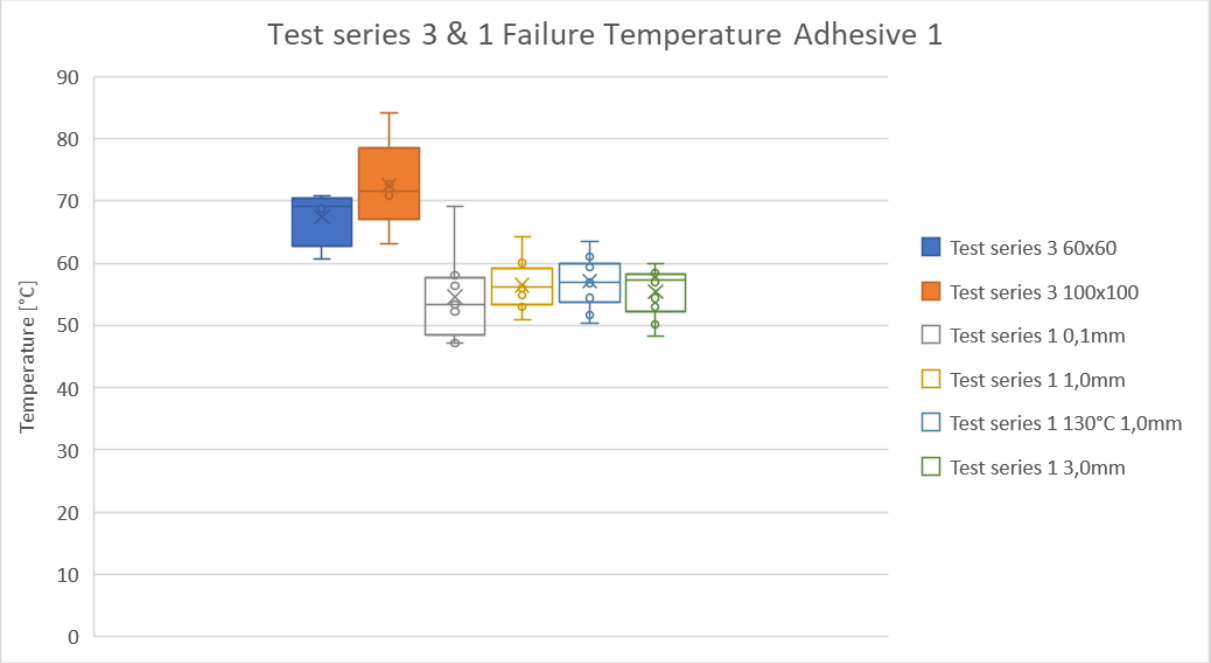

Figure 17: Comparison of failure temperatures of test series 3 (creep tests with glued in rods) and test series 1 (small scale tension shear tests) for Adhesive 1 with a load level of 40 % of the reference tests

A similar result is shown for Adhesive 2 (see Figure 18). The failure temperatures are in the range of approx. 80 °C to 90 °C for test series 3 and are therefore higher than for Adhesive 1. The same results were achieved in test series 1. For Adhesive 2 the difference between test series 3 and especially the glue line thickness of 0.1 mm and 1.0 mm of test series 1 are not as high as for Adhesive 1.

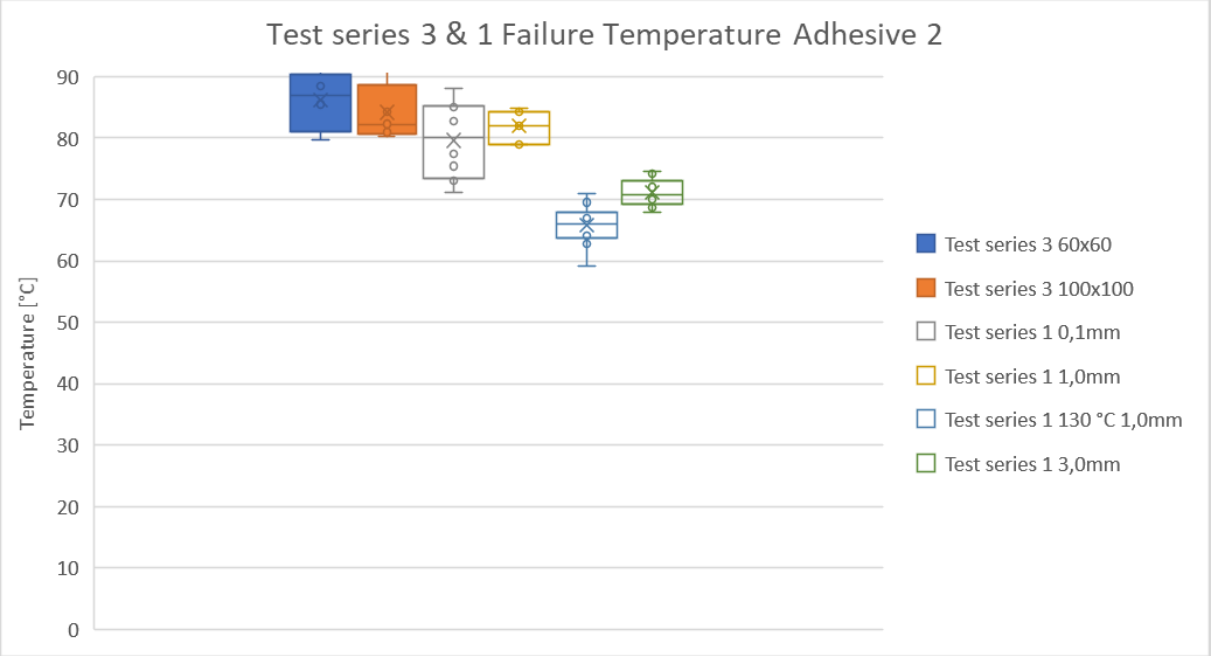

Figure 18: Comparison of failure temperatures of test series 3 (creep tests with glued in rods) and test series 1 (small scale tension shear tests) for Adhesive 2 with a load level of 40 % of the reference tests

When comparing the test specimens with a higher mechanical tensile load of 60% of the loads achieved from the reference tests, the failure temperatures of Adhesive 1 are in the range of approx. 64 °C - 70 °C (see Figure 19). It can be seen that the load level applied has a big influence on the failure temperature. However, only a small number of tests were carried out for this series, which is why there is no large scattering like in test series 3.2. The failure temperatures are higher than that for test series 1 which may be caused by the earlier described relative load level applied in the tests. For test series 1 the glue line thickness of 3.0 mm wasn`t tested with this load level due to immediate failure of the specimen when the load was applied.

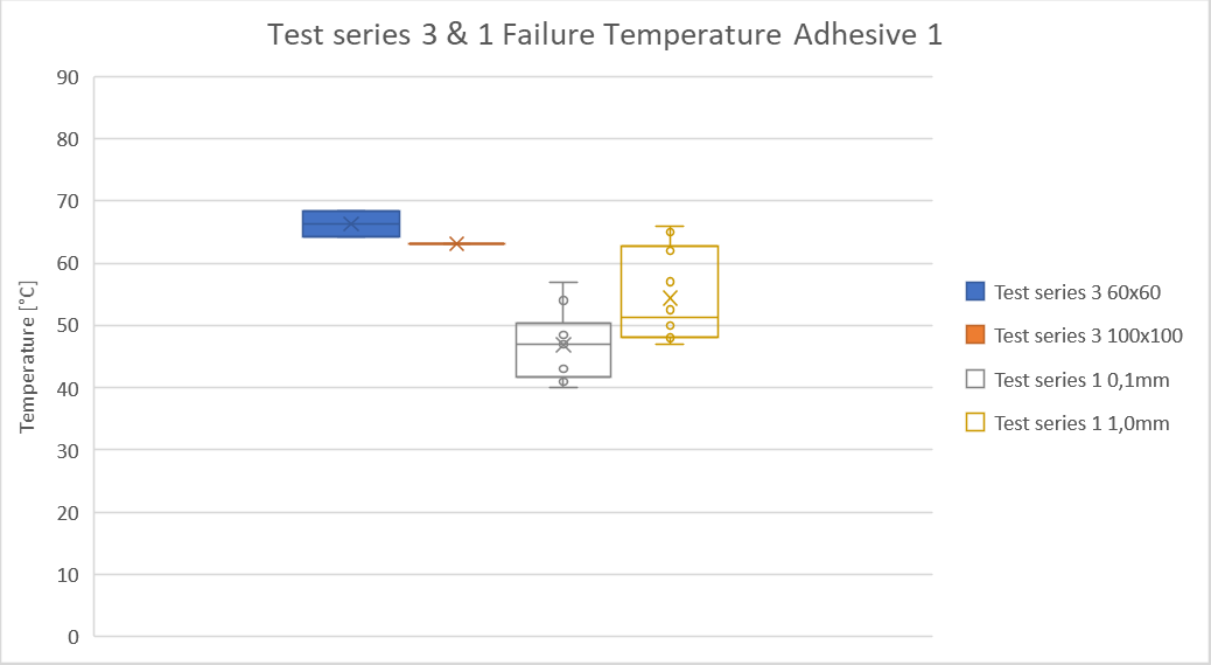

Figure 19: Comparison of failure temperatures of test series 3 (creep tests with glued in rods) and test series 1 (small scale tension shear tests) for Adhesive 1 with a load level of 60 % of the reference tests

Adhesive 2 shows a similar behavior (see Figure 20). The failure temperature is lower for the higher load level of 60 % of the reference tests. The failure temperatures lie within a range of approx. 68 °C and 85 °C. This result is consistent with test series 1, in which faster failure can occur due to a higher load. The difference in failure temperatures in test series 3 showed no direct correlations for the two cross-sections. Further diagrams are given in Appendix F.

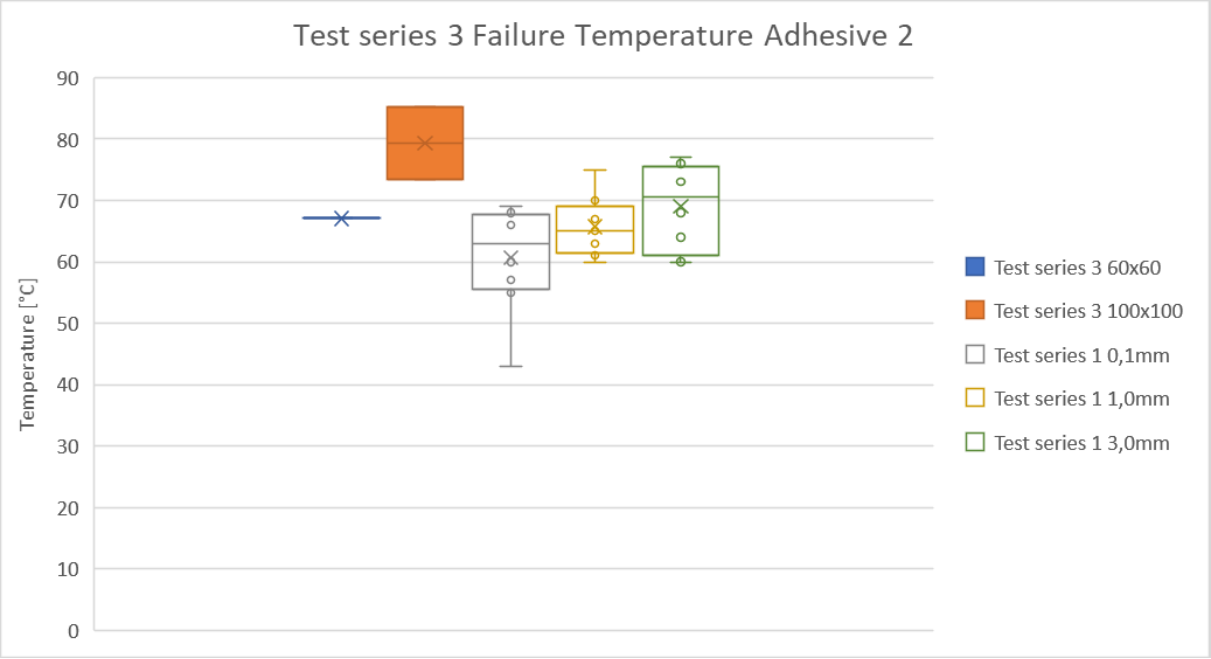

Figure 20: Comparison of failure temperatures of test series 3 (creep tests with glued in rods) and test series 1 (small scale tension shear tests) for Adhesive 2 with a load level of 60 % of the reference tests

2.3.2 Influence of the joint width

In test series 3.4, the joint was carried out with a planned gap of 2 mm. The test specimens are compared with test specimens of the test series 3.2 which were identical in construction. Figure 21 shows the failure temperatures for the four measurement points of each specimen. The results show that Adhesive 1 has lower failure temperatures and therefore a lower thermal resistance.

The failure temperatures for test series 3.2 and 3.4 are very similar for all measuring points regardless of the adhesive type (see Figure 21). The failure times are also in a similar range which is why it can be assumed that a joint gap smaller than 2 mm has no influence whatsoever on the heating behavior of the rod (see also the Appendix G).

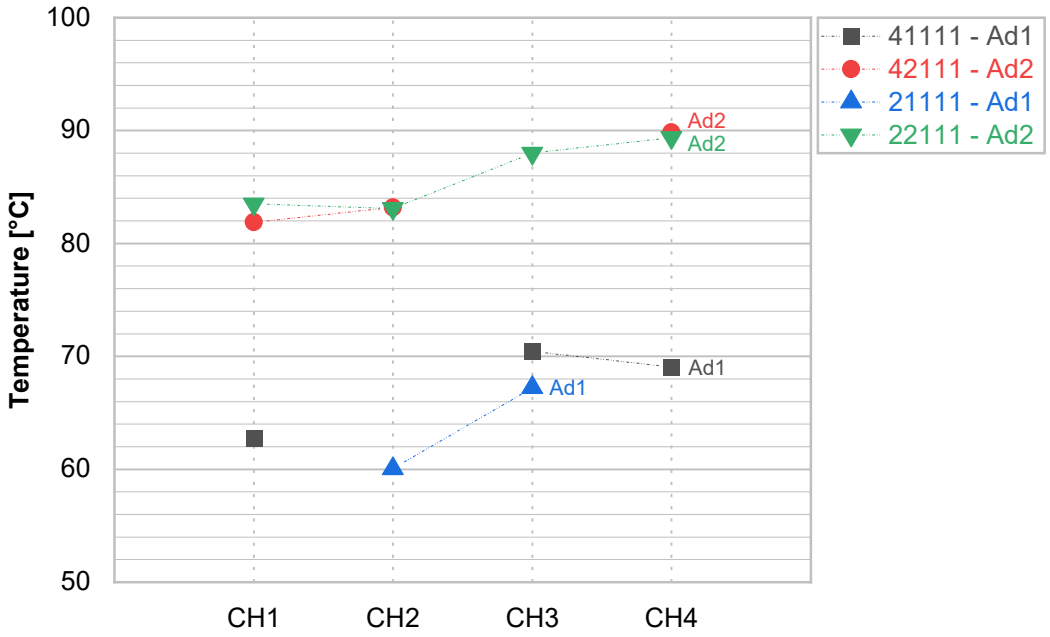

Figure 21: Comparison of failure temperatures of test series 3.2 and test series 3.4 for identical specimen configurations except of the joint between the two specimen halves

2.3.3 Influence of the glue line thickness

Figure 22 shows a comparison of the glue line thickness of the thermally loaded test specimens from test series 3.2. The identical test specimens are listed one below the other in the legend. They differ only in the glue line thickness of 1 mm and 3 mm. Since the failure temperature is displayed here, the lower timber cover of the rod resulting from the same cross-section used has no role in the assessment.

The measurements always show a lower failure temperature for the 3 mm glue line thickness. This could be related to the higher load applied to the specimens. Relatively speaking, these are also subjected to a 40% load from the reference tests. In the case of the test specimens with a glue line thickness of 3 mm, higher failure loads were always achieved in the reference tests. In the case of the cross-sections of 60 mm x 60 mm these values were around 5 % higher on average, and in the case of the cross-sections of 100 mm x 100 mm, values that were 20% higher on average were achieved. It was assumed that a reduction in stress peaks at

the borehole ends due to the larger glue line thickness occurred, resulting in the higher failure loads. The adhesive itself does not have a higher strength due to the larger glue line thickness. This strength and the residual load-bearing capacity are reduced as the temperature rises. It has already been confirmed by test series 1 (small scale tension shear tests) that greater mechanical stress leads to lower failure temperatures. The reason for this is that the residual load-bearing capacity of the adhesive is exceeded more quickly. Since the adhesive strength is the same for both glue line thicknesses, but a comparatively higher mechanical load is assumed for a joint thickness of 3 mm, the decreasing load-bearing capacity of the adhesive is exceeded more quickly when heated. It therefore seems plausible that with the larger glue line thicknesses, lower failure temperatures are achieved compared to the structurally identical counterparts with a glue line thickness of 1 mm.

When examining the failure times, it is apparent that the larger glue line thickness led to earlier failure of the test specimens. On the one hand, the reason for this could be the already mentioned higher load on the test specimens, which could more quickly exceed the residual load-bearing capacity of the adhesive. On the other hand, the test specimens had less wood covering the rod, which can lead to a faster temperature rise at the edge of the borehole (for the failure times see also Appendix G). The adhesive type had no influence on this behavior.

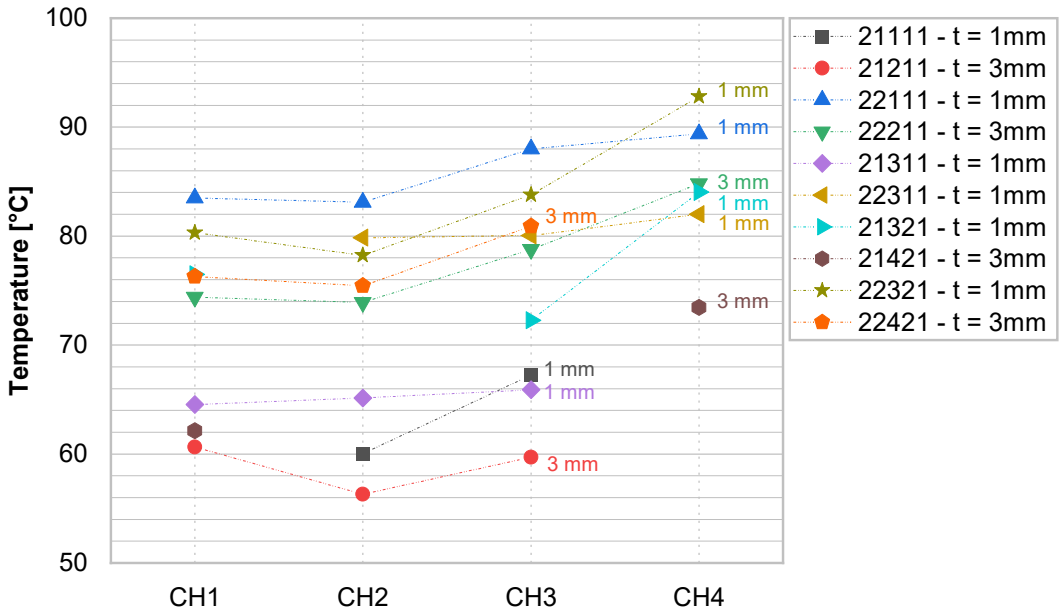

Figure 22: Comparison of failure temperatures of test series 3.2 for different glue line thicknesses

2.3.4 Influence of the thermocouple position

The test specimens were aligned in the same way in the thermal box. However, due to the manufacturing process, some had their thermocouples on the top surface, while others had their thermocouples turned sideways.

Figure 23 shows the temperature of the CH3 and CH4 for different specimens of test series 2.2 – 2.4. The air temperature curves of the test specimens selected are almost congruent and thus enable a good comparison of the thermal curves inside the component. There are no

signs that the position had a major influence on the temperature development in the test specimen (see Figure 23).

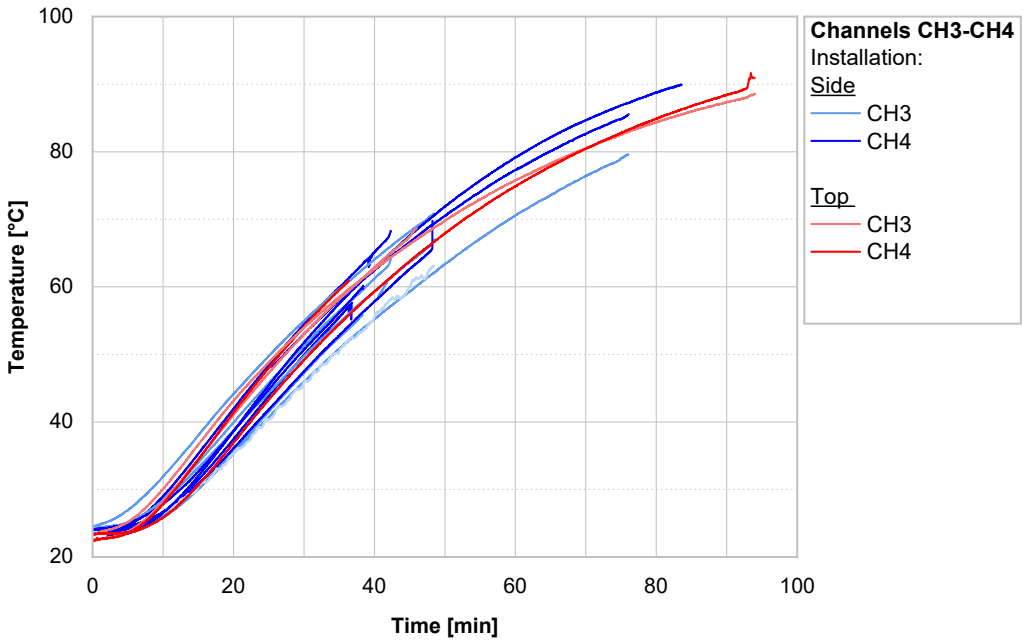

Figure 23:Temperature development in CH3 and CH4 for the positions on the side and on the top of the specimen (Side: SP 21211, 22211, 31111, 32111, 41111, 42111. Top: 21111, 22111) [1]

2.3.5 Deformation

The test setup only allowed the measurement of the total deformation of the test specimen. However, since the test specimens always failed on the side of the inlet in the thermo box, it is assumed that a large part of the recorded deformation took place in this area.

Two typical deformation curves are shown in Figure 24. The deformation, temperature and mechanical load are given on the vertical axis. On the horizontal axis the duration of the tests is applied. The left diagram shows the curve for Adhesive 1 and the right one for Adhesive 2. On the x-Axis the time of failure as well as the starting time of the deformation are marked.

The deformation curves can generally be divided into four sections. At the beginning there is a steep ascent in which the load is brought up to the target level. A plateau then forms in which the deformation hardly changes. The fluctuations that occur are attributed to the loss of pressure in the hydraulic system and therefore had to be readjusted during the tests. In the third section, the adhesive softens and the deformation increases in a quasi-linear manner. However, the load level can still be maintained. This increase lasts until phase four, which is accompanied by a sudden increase in deformation. In this case, the applied load can no longer be transferred by the adhesive and the test specimen suddenly fails.

A different behavior can be observed in Section 3 for the two adhesives. Adhesive 1 shows a significantly shorter time to failure in all test specimens. The increase in deformation is also steeper and the test specimen deforms more quickly and more severely. In the case of Adhesive 2, deformation begins at lower temperatures. However, a flatter rise can also be seen. Here the adhesive deformation occurs over a longer period of time until a critical temperature is exceeded and the adhesive fails. The reason could be the higher thermal resistance of Adhesive 2. When subjected to the effects of temperature, it retains a greater proportion of its

load-bearing capacity in comparison to Adhesive 1. For this reason, the reduced strength because of the thermal load could already lead to the first deformations in the adhesive. However, the carrying capacity limit has not yet been exceeded.

Based on test series 1, Adhesive 1 already shows a strong reduction in strength when reaching a temperature of 60 °C which is why there are no large load-bearing reserves left. Therefore, faster and larger deformations occur until failure. The load-deformation curves of the other specimens are shown in Appendix G.

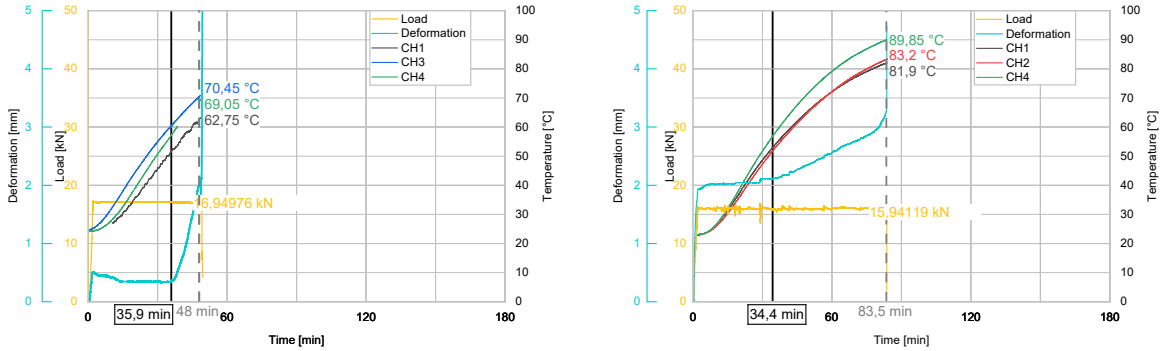

Figure 24: Typical load-deformation curves for Adhesive 1 (left) and Adhesive 2 (right) [1]

2.3.6 Temperature limit

The tests showed that the adhesive should not exceed a specific temperature to ensure its load-bearing capacity. Therefore, a critical temperature limit is derived from the failure temperatures in test series 3.

As stated in chapter 2.5, the required load level is around 37 % between the characteristic load-bearing capacities in the event of fire and at ambient temperature.

The value of the calculated characteristic load-carrying capacity according to EN 1995-1-1 is significantly lower than the loads applied in the tests (see Table 3). For this reason, the failure temperature from the tests with a load level of 40 % of the reference tests is used to determine the critical temperature limit. Because of the uneven temperature distribution in the oven only the values of CH3 and CH4 were considered in the calculation. Also, only the tests in which an adhesive failure was present were considered for the determination of the temperature limit. The 20 % - fractile value was used for the case of fire.

The critical temperature limit based on these tests is 69 °C for Adhesive 1 and 79 °C for Adhesive 2. The temperatures were rounded down to the nearest integer value.

The mean temperatures depending on the load level are given in Appendix H.

Table 5: Critical temperature limit based on test series 3 for specimens which failed in the glue line and for a load level of 40 % of the reference load

	Adhesive 1	**Adhesive 2**
0,4 F_{mean}	[°C]	[°C]
5%-Quantile	63	75
20%-Quantile	69	79

3 Summary and conclusion

In test series 3 two different test setups were carried out. In the reference test the specimens were loaded mechanically under tensile stresses until failure. From these tests the load levels for the specimens in setup 2 were derived.

In setup 2 creep tests under thermal load were performed. The mean values calculated from the reference tests were factored with 0.4 and 0.6 and applied as a mechanical load in the creep tests. Afterwards a thermal load of 110 °C was applied.

The results from the reference tests were compared with various design methods. The design according to EN 1995-1-1 shows significantly lower pull-out resistances than that were achieved in the tests and are therefore on the safe side.

Basically, the reference tests with wood cross-sections of 60 mm × 60 mm did not allow any conclusions about the influence of certain configurations, since they all failed under a similar load. The small differences are presumably due to the inhomogeneities in the wood, since failure only occurred there.

With the larger cross-sections of 100 mm x 100 mm, it was shown that thicker glue lines at ambient temperature have a positive effect on the pull-out resistance. Better stress distribution in the adhesive joint is assumed here, which reduces the stress peaks at the respective borehole ends. The opposite effect was observed in the temperature loaded tests. Here, the glue line thickness of 1 mm shows higher failure temperatures. The reason for this is considered to be the determination of the load level. Since a higher failure load was achieved with a glue line thickness of 3 mm in the reference tests, this was applied proportionately to the creep tests. However, the strength or load-bearing capacity of the adhesive does not increase with increasing glue line thickness. Since the adhesive loses its load-bearing capacity under the influence of temperature, a higher load at the beginning leads to earlier failure of the connection or to lower failure temperatures. Also, due to the bigger borehole diameter the cover of the rod was reduced which leads to a faster heating of the adhesive at the borehole edge.

The two types of adhesive showed different failure behavior under the influence of temperature. For example, in the case of Adhesive 2, similar to test series 1, higher adhesive temperatures were measured. In addition, the two adhesives differed in their deformation behavior. In the case of Adhesive 2, a longer creep behavior can be observed up to the final point of failure. In the case of Adhesive 1, however, the initiation of the creep mechanism soon leads to the failure of the test specimen. It is assumed that the greater reduction in load-bearing capacity of Adhesive 1 under thermal load (see also test series 1) is responsible for this behavior. When the critical temperature limit is exceeded, there are hardly any load reserves, which is why no distinctive creep process can occur.

The joint between the two specimen halves with a gap of 2 mm thickness showed no different heating behavior with the specimen without the gap. It is therefore assumed that no increased heat input into the connection can be assumed for this width of the joint.

Based on the tests carried out, failure of the adhesive in the connection is assumed in the event of a fire. Based on the tests with a 40% mechanical load from the reference tests, the critical adhesive temperature limit was determined, which should not be exceeded in order to prevent the test specimen from failing. Here the 20 % - fractile value was used. This results in a critical temperature limit of 69 °C for Adhesive 1 and 79 °C for Adhesive 2.

Due to the furnace design, it was not possible to distribute the heat evenly along the test specimen. For this reason, only two of the four temperature measuring points distributed in the test specimen were ultimately used for the assessment of the failure temperature. These points were in the warmer area of the thermal box next to the inlet. On this side of the specimen the pull-out occurred for every creep test under thermal load.

The execution of the test did not allow any statement as to whether the deformations are of a plastic nature at the beginning or whether they decrease again when the temperature is reduced. An increase in the glass transition temperature of the adhesive could not be determined. In the event of a fire, it is therefore assumed that this effect has no role in the strength development of the connection. A follow-up examination of the strength development after a cooling process would be desirable. However, it can be assumed that the glass transition temperature of the adhesive can be increased by appropriate pre-treatment and that the level of the critical adhesive temperature limit can also be increased to this level.

The evaluation of the critical adhesive temperature limit was based on the two adhesives used. These are not representative of all adhesives that are of the same type as the components and chemical composition vary by manufacturer. Further tests are therefore necessary to determine the critical adhesive temperature limit of other adhesives, since general applicability is not given.

In construction practice, individual steel rods are rarely glued in and even the small wood cross-section of 60 mm × 60 mm has hardly any areas of application. The minimum possible edge distances according to EN 1995-1-1 were applied here in order to check whether there is sufficient thermal protection in the event of fire. The use of a single bar makes it easier to assess the load-bearing capacity, since groups of bars do not achieve even load distribution due to inaccuracies during installation (skewing boreholes, wood errors, bubbles in the glue line, etc.).

Another aspect that was not considered is the permanent thermal load on the adhesive in the area of the critical temperature limit and the impact on the load-bearing capacity or fatigue of the adhesive.

References

[1] DORBATH, T.: *Warmkriechversuche – Verhalten von eingeklebten Gewindestangen unter Temperaturbeanspruchung*. München, TUM, Lehstuhl für Holzbau und Baukonstruktion. Masters Thesis. 02/2022

[2] *DIN EN 1995-1-1:2010-12, Eurocode_5: Bemessung und Konstruktion von Holzbauten_- Teil_1-1: Allgemeines_- Allgemeine Regeln und Regeln für den Hochbau; Deutsche Fassung EN_1995-1-1:2004_+ AC:2006_+ A1:2008*

[3] *DIN EN 1995-1-2:2010-12, Eurocode_5: Bemessung und Konstruktion von Holzbauten_- Teil_1-2: Allgemeine Regeln_- Tragwerksbemessung für den Brandfall; Deutsche Fassung EN_1995-1-2:2004_+ AC:2009*

[4] *DIN EN 1990:2021-10, Eurocode: Grundlagen der Tragwerksplanung; Deutsche Fassung EN_1990:2002_+ A1:2005_+ A1:2005/AC:2010*

[5] WERTHER, N. ; GRÄFE, M. ; HOFMANN, V. ; WINTER, S.: *Untersuchungen zum Brandverhalten von querkraftbeanspruchten Verbindungen bei Holzbaukonstruktionen, Neuentwicklung und Optimierung von Verbindungssystemen und allgemeinen Konstruktionsregeln*. 2015 (Schlussbericht F 2938)

[6] *DIN EN 14358:2016-11, Holzbauwerke_- Berechnung und Kontrolle charakteristischer Werte; Deutsche Fassung EN_14358:2016*

A Density

Table 6: Density of tests series 3.1

SP	Density [kg/m³]	
	V	H
11111	452,1	457,3
11112	449,8	453,8
11211	492,6	453,6
11212	468,5	456,5
12111	463,5	459,9
12112	434,7	461,3
12211	471,3	463,2
12212	472,0	452,2
11311	439,3	427,5
12311	444,1	445,6
11321	440,4	427,4
11322	422,3	436,6
11421	448,8	421,7
11422	431,2	431,6
12321	457,2	441,6
12322	425,8	453,4
12421	434,0	448,1
12422	432,3	429,5

B Moisture content

Table 7: Density and moisture content of test series 3.2 – 3.4

Specimen	Dry density	Density according to EN 408	Density Sample	Deviation	Density Sample after Test	Moisture content	Moisture content after test
21111-V	399,9	468,4	458,1	2%	441,8	12,9	10,5
21111-H	412,5	448,6	444,8	1%	453,8		10,0
21211-V	416,9	458,3	437,6	5%	459,0	14,8	10,1
21211-H	395,0	473,4	463,0	2%	430,6		9,0
22111-V	403,4	463,6	463,2	0%	440,8	12,1	9,3
22111-H	420,0	459,3	446,8	3%	457,2		8,9
22211-V	447,6	499,2	494,9	1%	488,1	11,1	9,1
22211-H	440,8	487,6	486,3	0%	480,5		9,0
21311-V	391,2	449,8	436,6	3%	430,3	13,3	10,0
21311-H	395,2	441,1	434,3	2%	429,8		8,8
22311-V	380,4	431,7	416,5	4%	415,8	14,1	9,3
22311-H	377,9	433,5	421,9	3%	408,1		8,0
21321-V	398,5	428,6	422,9	1%	438,3	12,6	10,0
21321-H	383,6	451,8	442,9	2%	415,7		8,4
21421-V	390,8	435,1	425,5	2%	431,3	12,5	10,3
21421-H	384,0	436,2	433,8	1%	418,7		9,0
22321-V	377,7	429,8	418,8	3%	413,4	13,3	9,5
22321-H	387,0	436,9	425,9	3%	416,4		7,6
22421-V	386,2	439,9	428,0	3%	421,8	13,3	9,2
22421-H	382,7	431,1	422,4	2%	413,6		8,1
31111-V	405,7	439,8	450,7	-2%	446,1	10,9	11,1
31111-H	407,1	461,2	452,5	2%	446,1		11,2
32111-V	402,4	449,0	447,9	0%	443,4	9,3	11,3
32111-H	430,5	461,5	476,8	-3%	468,7		10,8
31321-V	407,2	435,7	421,0	3%	450,2	13,1	11,2
31321-H	381,0	455,9	453,0	1%	414,0		10,5
32321-V	384,1	431,3	411,8	5%	422,5	14,5	11,1
32321-H	373,3	435,6	426,7	2%	402,8		10,3
41111-V	454,44	482,2	471,8	2%	448,1	12,43	11,0
41111-H	471,83	457,8	454,4	1%	464,6		10,6
42111-V	491,22	470,4	460,7	2%	485,5	10,78	10,6
42111-H	460,69	485,1	491,2	-1%	450,7		10,1

C Details gluing process

Table 8: Date of gluing

	Type	Specimen Half 1				Specimen Half 2 2			
		Borehole 1 (mid)		Borehole 2		Borehole 3 (mid)		Borehole 4	
11111	EP	29.03.2021	12:20-12:30	19.04.2021	13:40-13:50	29.03.2021	12:20-12:30	03.05.2021	13:00-13:10
11112	EP	29.03.2021	12:20-12:30	19.04.2021	13:40-13:50	29.03.2021	12:20-12:30	03.05.2021	13:00-13:10
11211	EP	30.03.2021	16:15-16:20	19.04.2021	13:40-13:50	30.03.2021	16:15-16:20	03.05.2021	13:00-13:10
11212	EP	30.03.2021	16:15-16:20	19.04.2021	13:40-13:50	30.03.2021	16:15-16:20	03.05.2021	13:00-13:10
12111	PUR	29.03.2021	12:20-12:30	19.04.2021	13:20-13:30	29.03.2021	12:20-12:30	26.04.2021	13:00-13:10
12112	PUR	29.03.2021	12:20-12:30	19.04.2021	13:20-13:30	29.03.2021	12:20-12:30	26.04.2021	13:00-13:10
12211	PUR	30.03.2021	16:15-16:20	19.04.2021	13:20-13:30	30.03.2021	16:15-16:20	26.04.2021	13:00-13:10
12212	PUR	30.03.2021	16:15-16:20	19.04.2021	13:20-13:30	30.03.2021	16:15-16:20	26.04.2021	13:00-13:10
11311	EP	22.04.2021	11:30-11:40	26.04.2021	13:20-13:30	22.04.2021	11:30-11:40	03.05.2021	13:00-13:10
12311	PUR	30.03.2021	16:30-16:40	20.04.2021	16:30-16:40	30.03.2021	16:30-16:40	26.04.2021	13:10-13:20
11321	EP	22.04.2021	11:30-11:40	26.04.2021	13:20-13:30	22.04.2021	11:30-11:40	03.05.2021	13:00-13:10
11322	EP	22.04.2021	11:30-11:40	26.04.2021	13:20-13:30	22.04.2021	11:30-11:40	03.05.2021	13:00-13:10
11421	EP	20.04.2021	16:10-16:20	22.04.2021	11:50-12:00	20.04.2021	16:10-16:20	26.04.2021	13:30-13:40
11422	EP	20.04.2021	16:10-16:20	22.04.2021	11:50-12:00	20.04.2021	16:10-16:20	26.04.2021	13:30-13:40
12321	PUR	30.03.2021	16:30-16:40	20.04.2021	16:30-16:40	30.03.2021	16:30-16:40	26.04.2021	13:10-13:20
12322	PUR	30.03.2021	16:30-16:40	20.04.2021	16:30-16:40	30.03.2021	16:30-16:40	26.04.2021	13:10-13:20
12421	PUR	20.04.2021	16:10-16:20	22.04.2021	11:50-12:00	20.04.2021	16:10-16:20	26.04.2021	13:10-13:20
12422	PUR	20.04.2021	16:10-16:20	22.04.2021	11:50-12:00	20.04.2021	16:10-16:20	26.04.2021	13:10-13:20
21111	EP	29.03.2021	12:20-12:30	19.04.2021	13:40-13:50	29.03.2021	12:20-12:30	03.05.2021	13:20-13:30
21211	EP	30.03.2021	16:15-16:20	19.04.2021	13:40-13:50	30.03.2021	16:15-16:20	03.05.2021	13:20-13:30
22111	PUR	29.03.2021	12:20-12:30	19.04.2021	13:20-13:30	29.03.2021	12:20-12:30	26.04.2021	13:00-13:10
22211	PUR	30.03.2021	16:15-16:20	19.04.2021	13:20-13:30	30.03.2021	16:15-16:20	26.04.2021	13:00-13:10
21311	EP	22.04.2021	11:30-11:40	26.04.2021	13:20-13:30	22.04.2021	11:30-11:40	03.05.2021	13:20-13:30
22311	PUR	30.03.2021	16:30-16:40	20.04.2021	16:30-16:40	30.03.2021	16:30-16:40	26.04.2021	13:10-13:20
21321	EP	22.04.2021	11:30-11:40	26.04.2021	13:20-13:30	22.04.2021	11:30-11:40	03.05.2021	13:20-13:30
21421	EP	20.04.2021	16:10-16:20	22.04.2021	11:50-12:00	20.04.2021	16:10-16:20	26.04.2021	13:30-13:40
22321	PUR	30.03.2021	16:30-16:40	20.04.2021	16:30-16:40	30.03.2021	16:30-16:40	26.04.2021	13:10-13:20
22421	PUR	20.04.2021	16:10-16:20	22.04.2021	11:50-12:00	20.04.2021	16:10-16:20	26.04.2021	13:10-13:20
31111	EP	29.03.2021	12:20-12:30	19.04.2021	13:40-13:50	29.03.2021	12:20-12:30	03.05.2021	13:20-13:30
32111	PUR	29.03.2021	12:20-12:30	19.04.2021	13:20-13:30	29.03.2021	12:20-12:30	26.04.2021	13:00-13:10
31321	EP	22.04.2021	11:30-11:40	26.04.2021	13:20-13:30	22.04.2021	11:30-11:40	03.05.2021	13:20-13:30
32321	PUR	30.03.2021	16:30-16:40	20.04.2021	16:30-16:40	30.03.2021	16:30-16:40	26.04.2021	13:10-13:20
41111	EP	29.03.2021	12:20-12:30	19.04.2021	13:40-13:50	29.03.2021	12:20-12:30	03.05.2021	13:00-13:10
42111	PUR	29.03.2021	12:20-12:30	19.04.2021	13:20-13:30	29.03.2021	12:20-12:30	26.04.2021	13:00-13:10

D Specimens after failure [1]

SP 11111

SP 11112

SP 11211

SP 11212

SP 12111

SP 12112

SP 12211

SP 12212

SP 11311

SP 12311

SP 11321

SP 11322

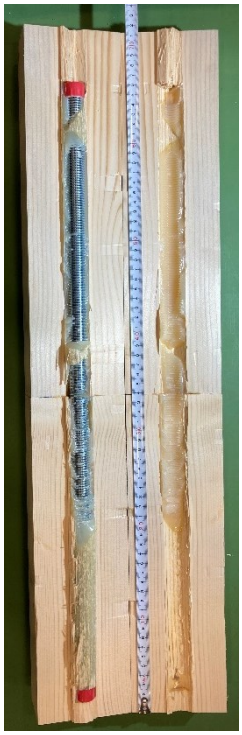

SP 11421

SP 11422

SP 12321

SP 12322

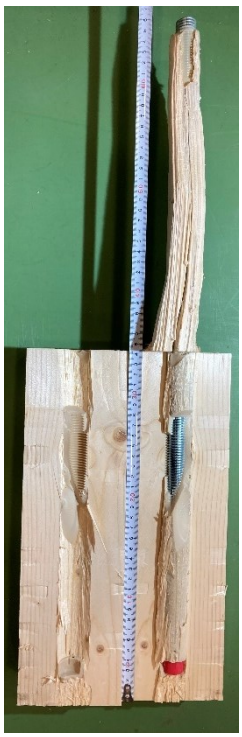

SP 12421

SP 12422

SP 21111

SP 21211

SP 22111

SP 22211

SP 21311

SP 22311

SP 21321

SP 21421

SP 22321

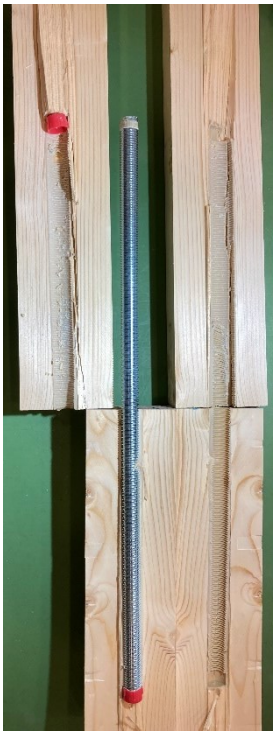

SP 22421

SP 31111

SP 32111

SP 31321

SP 32321

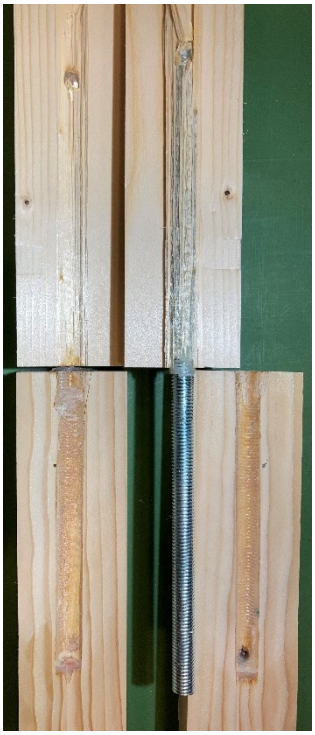

SP 41111

SP 42111

E Failure modes

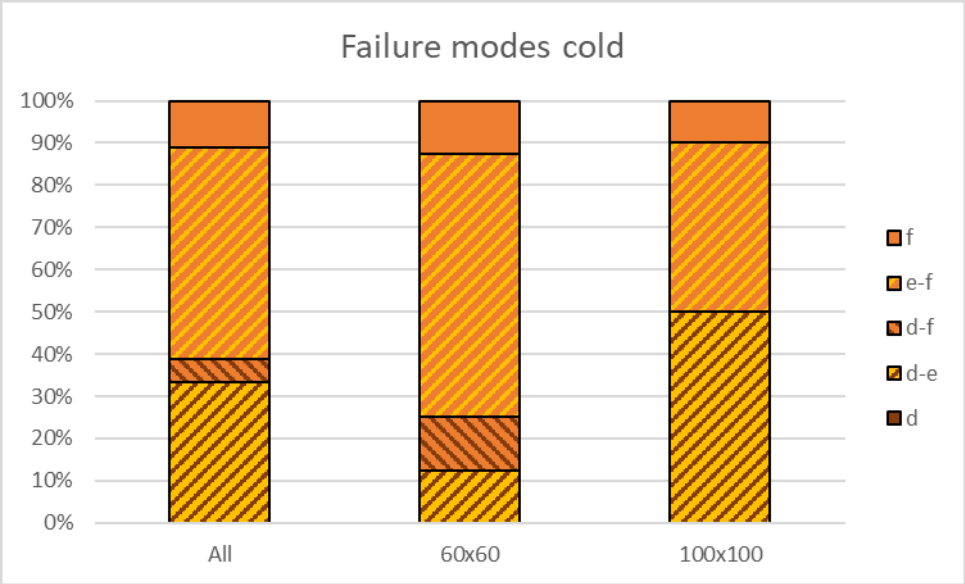

Figure 25: Failure modes for reference tests

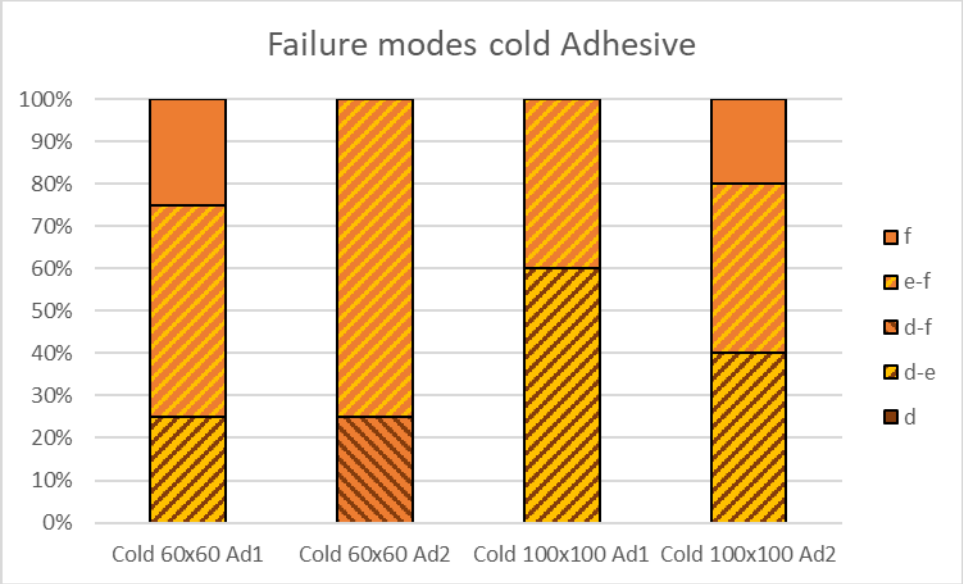

Figure 26: Failure modes for reference tests depending on the adhesive

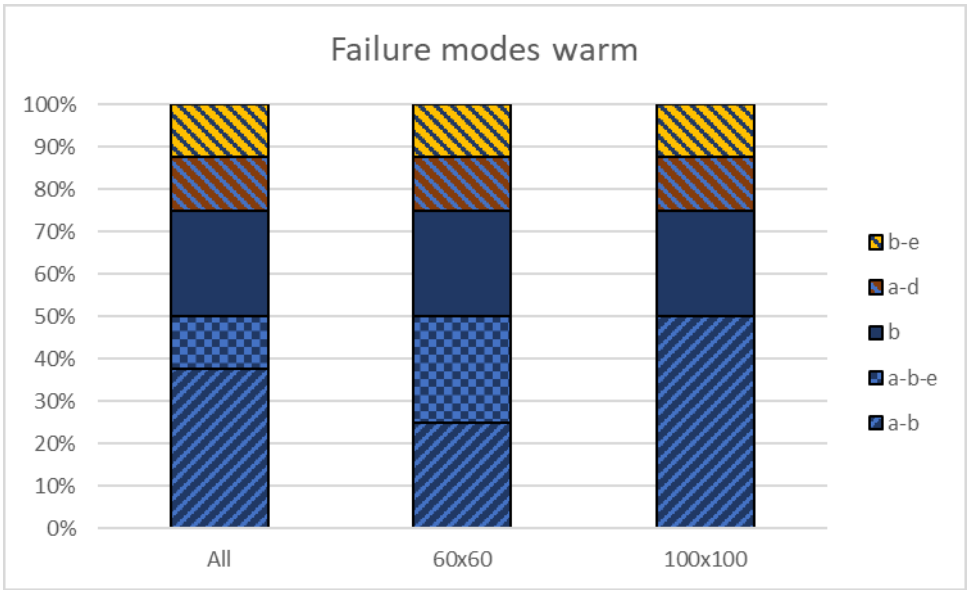

Figure 27: Failure modes for creep tests with thermal load

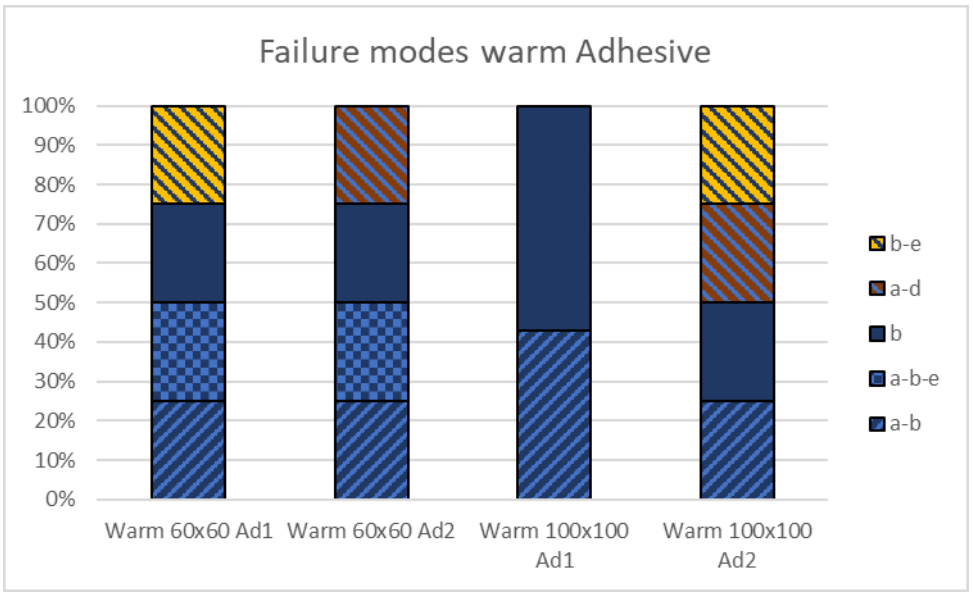

Figure 28: Failure modes for creep tests with thermal load depending on the adhesive

F Comparison test series 3 & 1

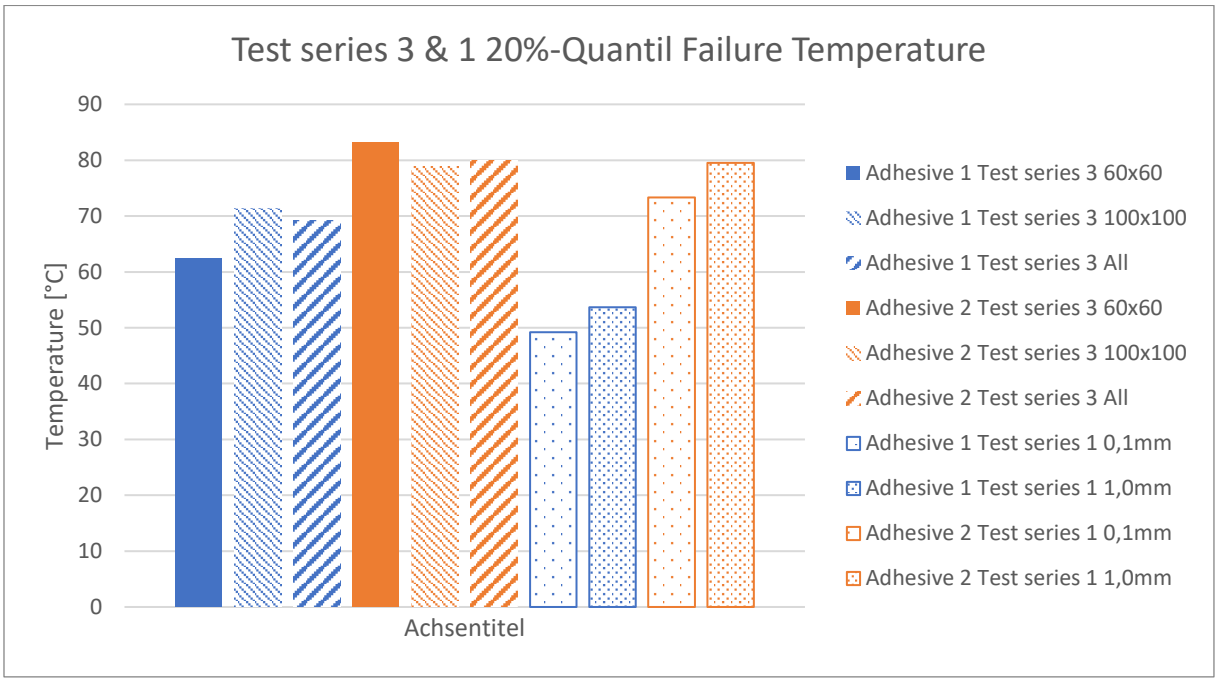

Figure 29: Comparison of failure temperatures of test series 3 and test series 1 for Adhesive 1 with a load level of 40 % of the reference tests

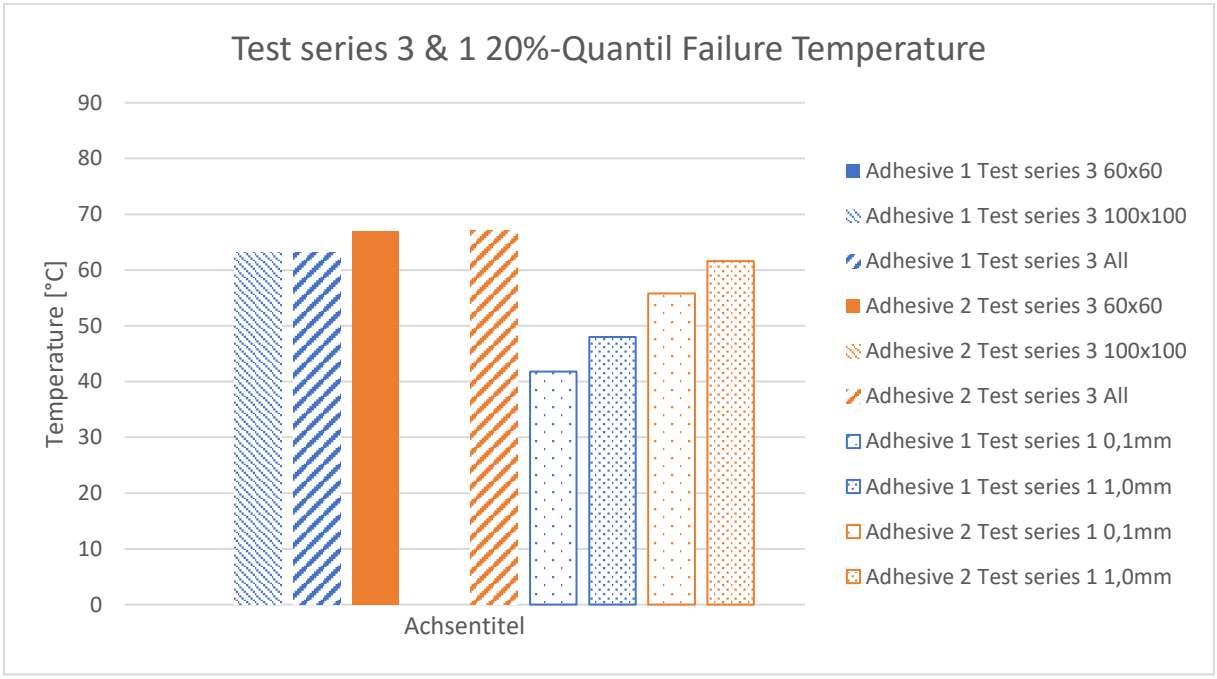

Figure 30: Comparison of failure temperatures of test series 3 and test series 1 for Adhesive 1 with a load level of 60 % of the reference tests

G Load-deformation curves

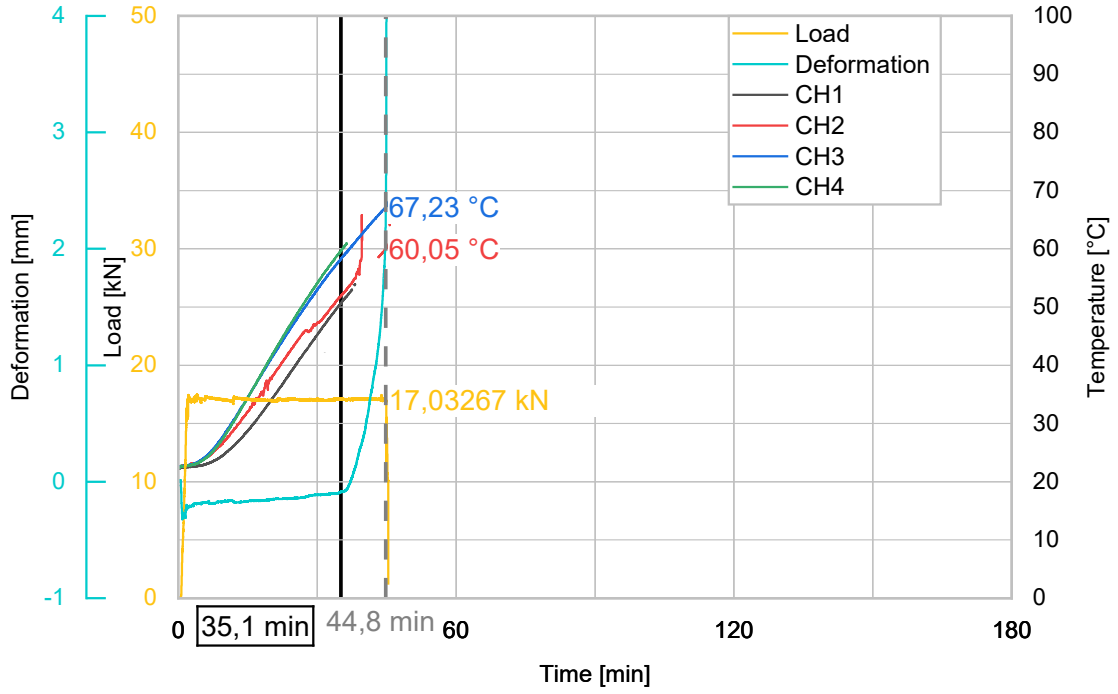

Figure 31: Load-deformation curve for specimen 21111

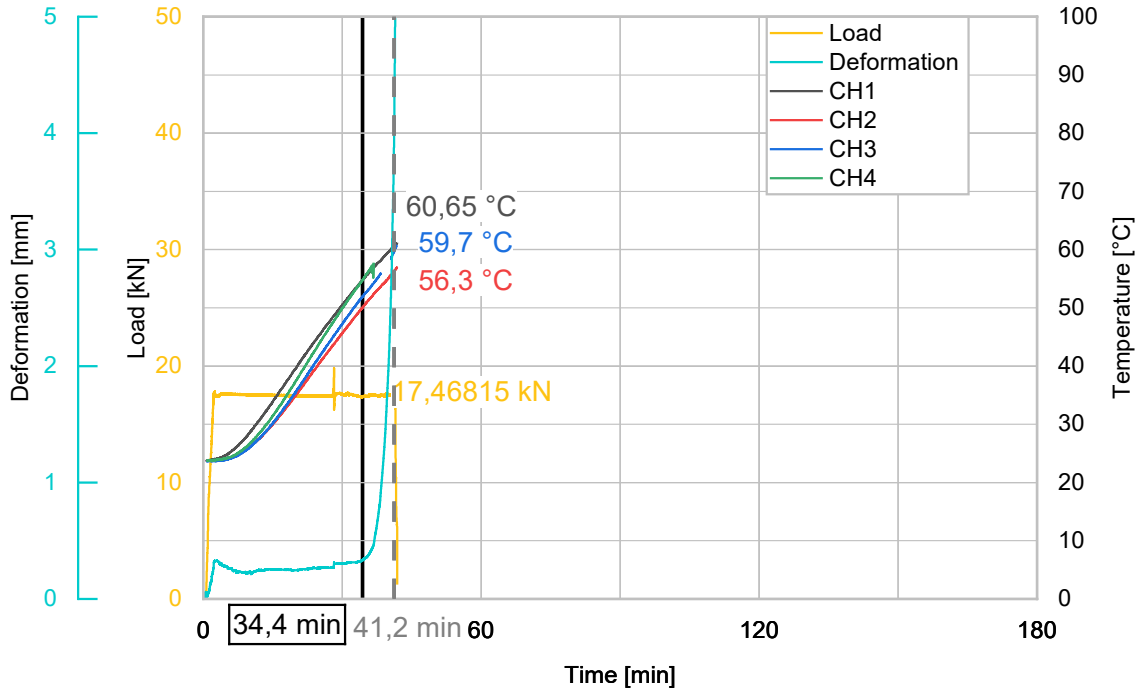

Figure 32: : Load-deformation curve for specimen 21211

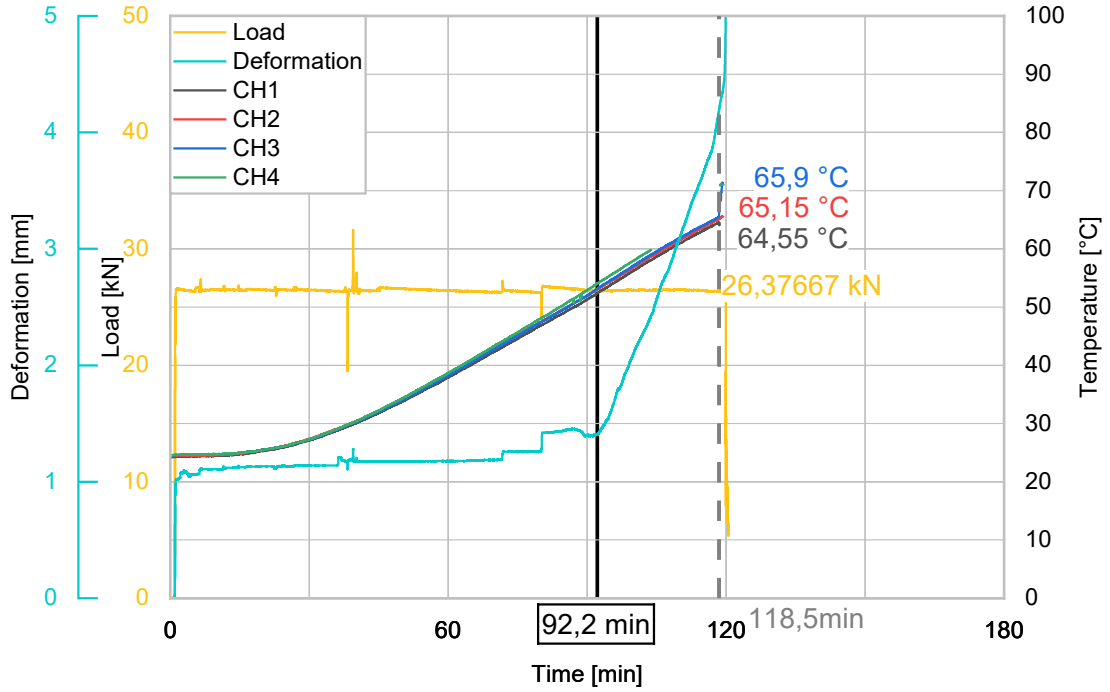

Figure 33: Load-deformation curve for specimen 21311

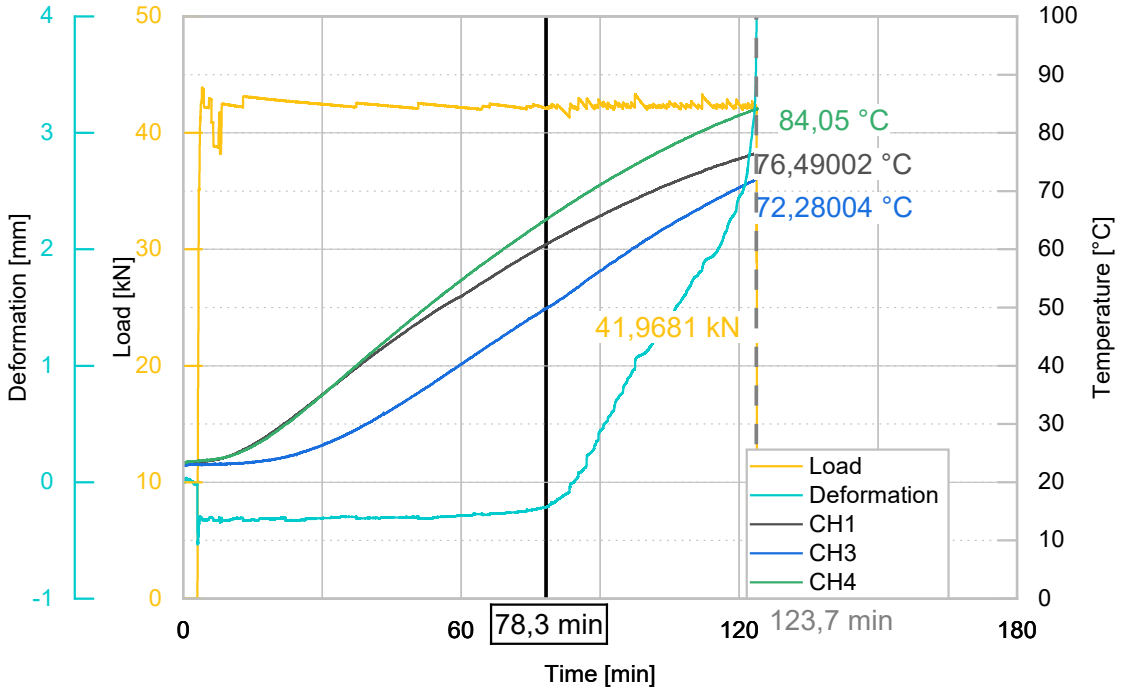

Figure 34: Load-deformation curve for specimen 21321

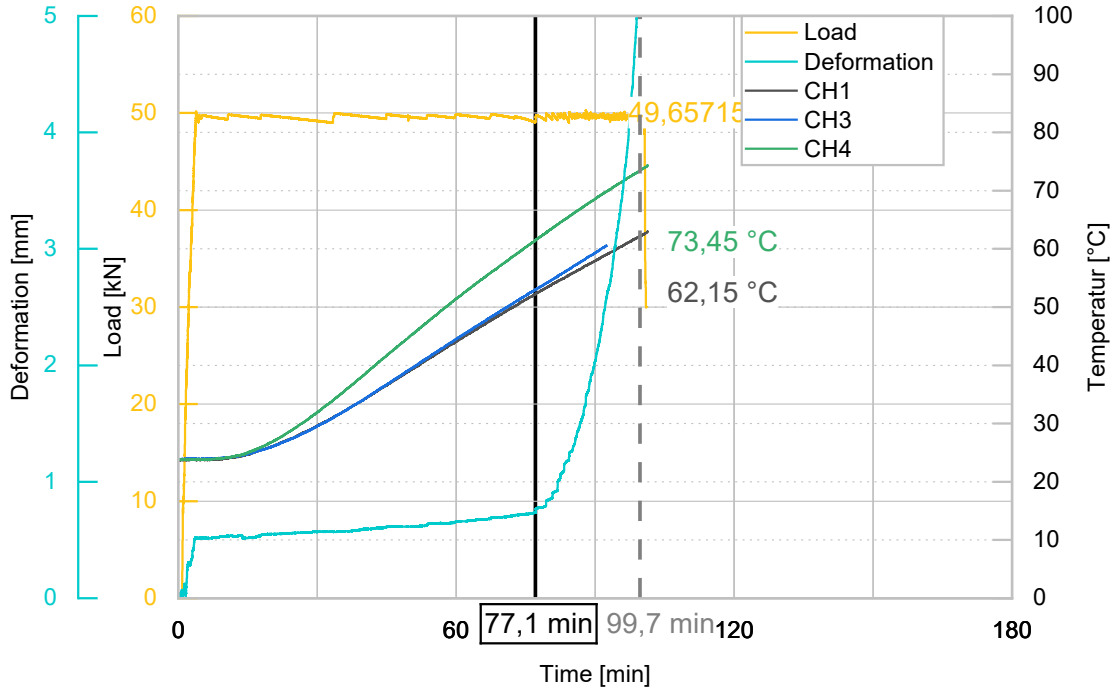

Figure 35: Load-deformation curve for specimen 21421

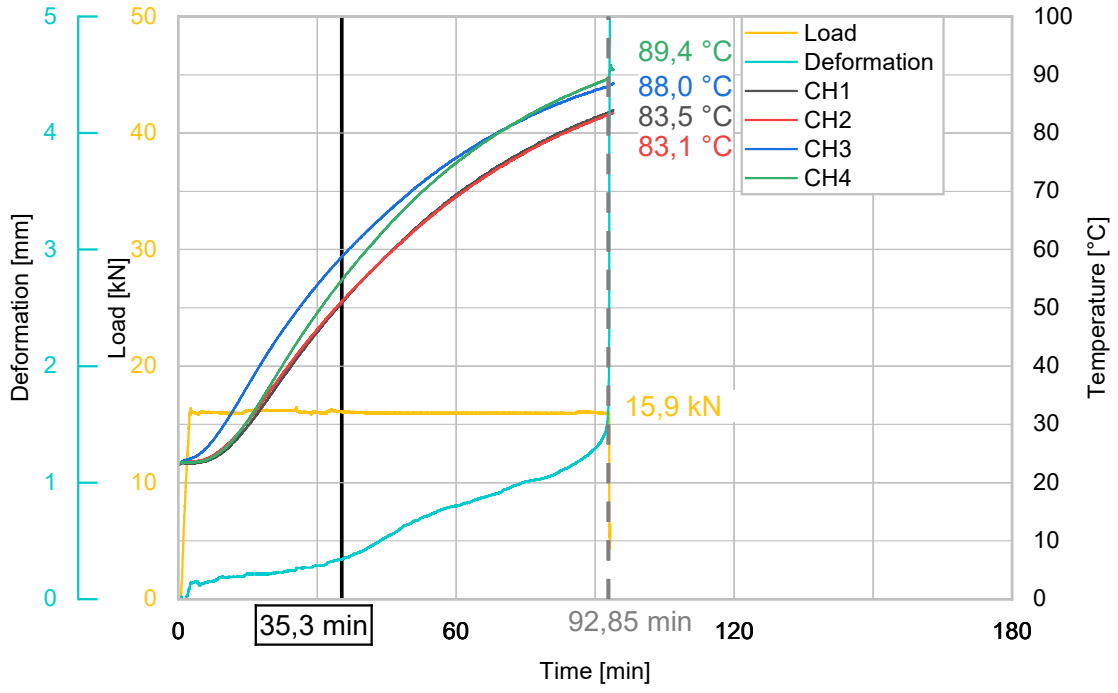

Figure 36: Load-deformation curve for specimen 22111

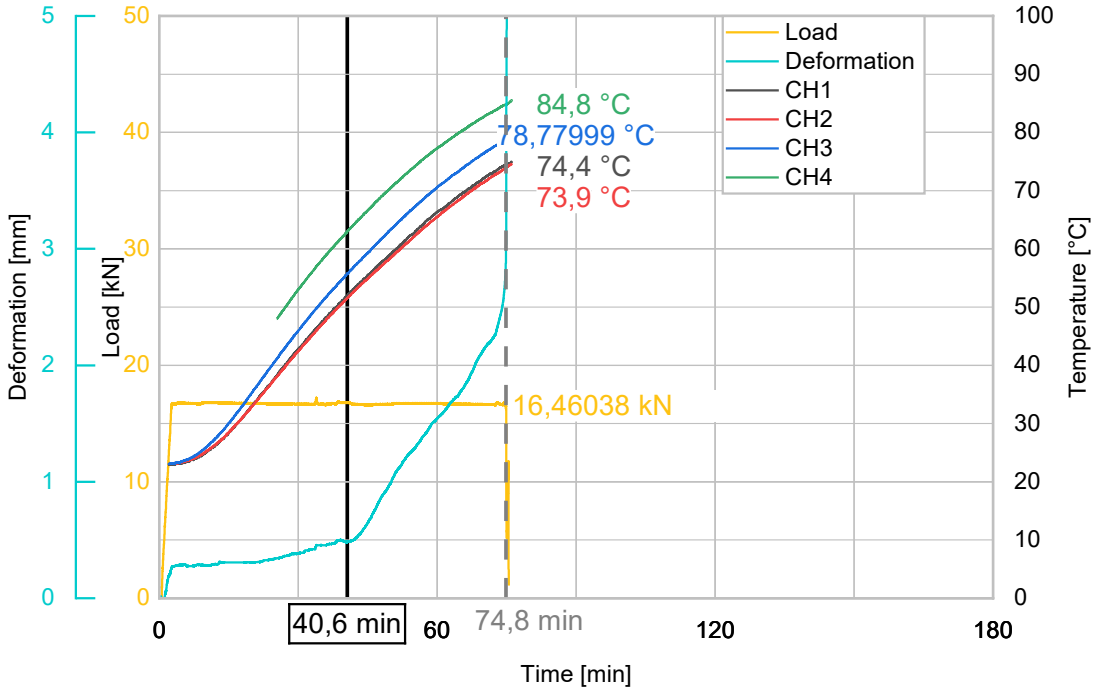

Figure 37: Load-deformation curve for specimen 22211

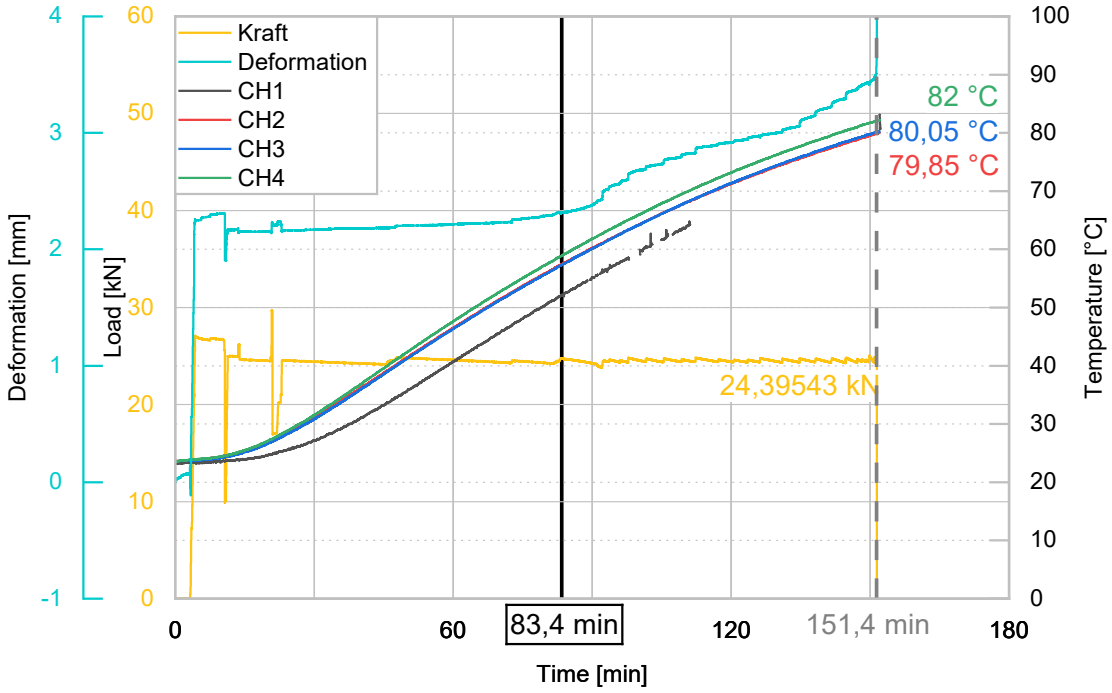

Figure 38: Load-deformation curve for specimen 22311

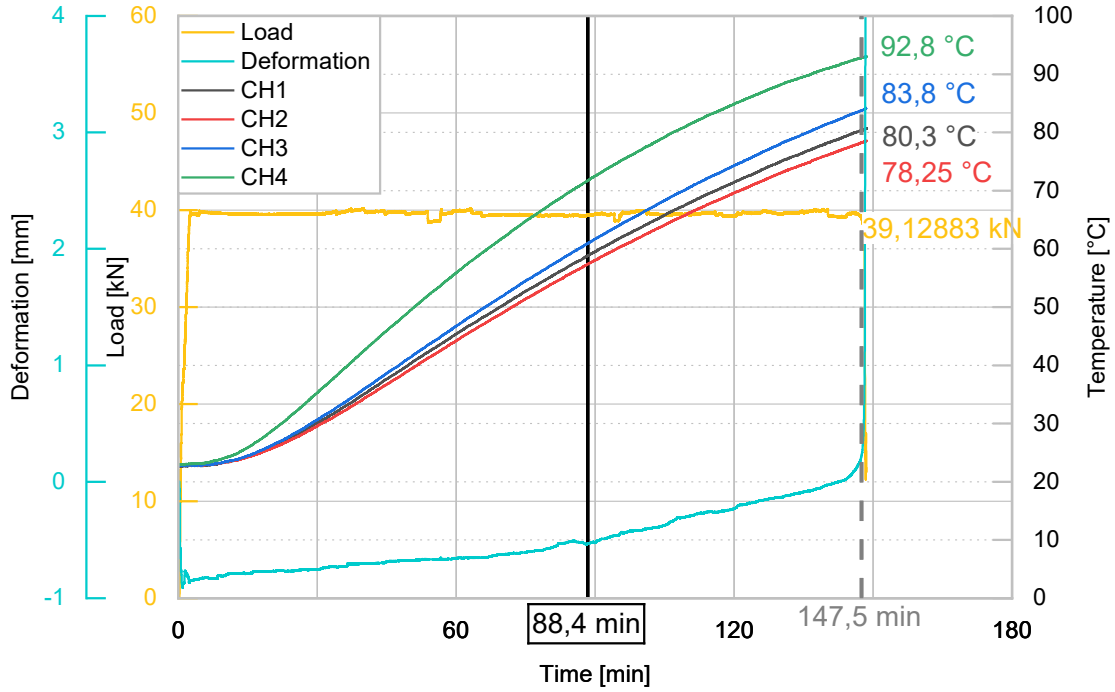

Figure 39: Load-deformation curve for specimen 22321

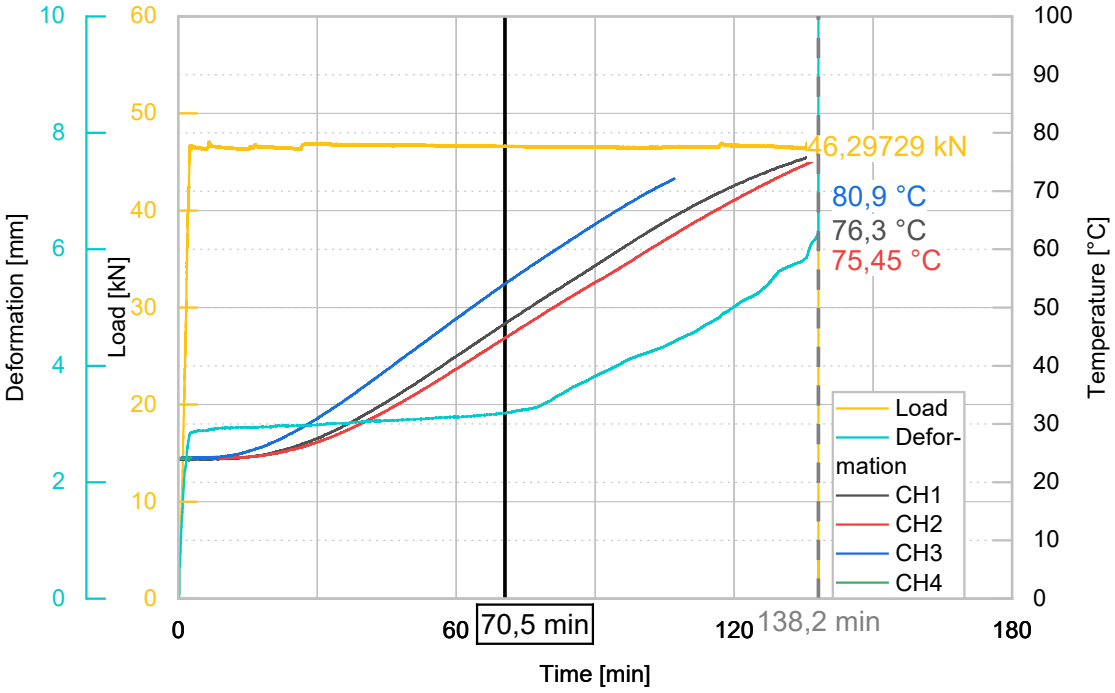

Figure 40: Load-deformation curve for specimen 22421

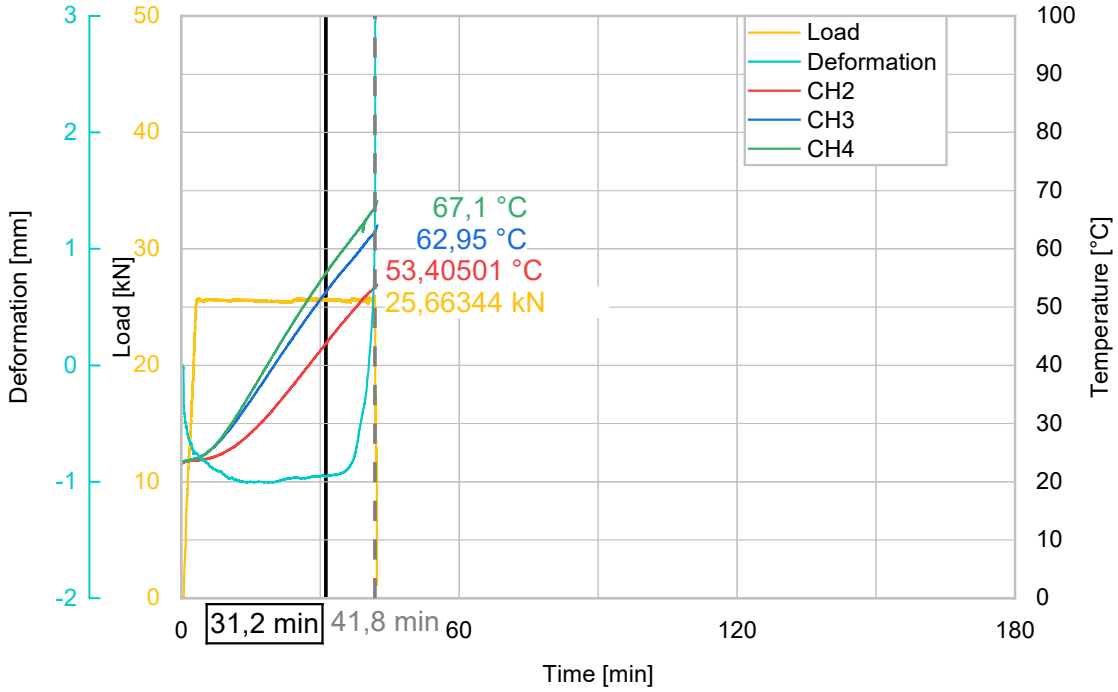

Figure 41: Load-deformation curve for specimen 31111

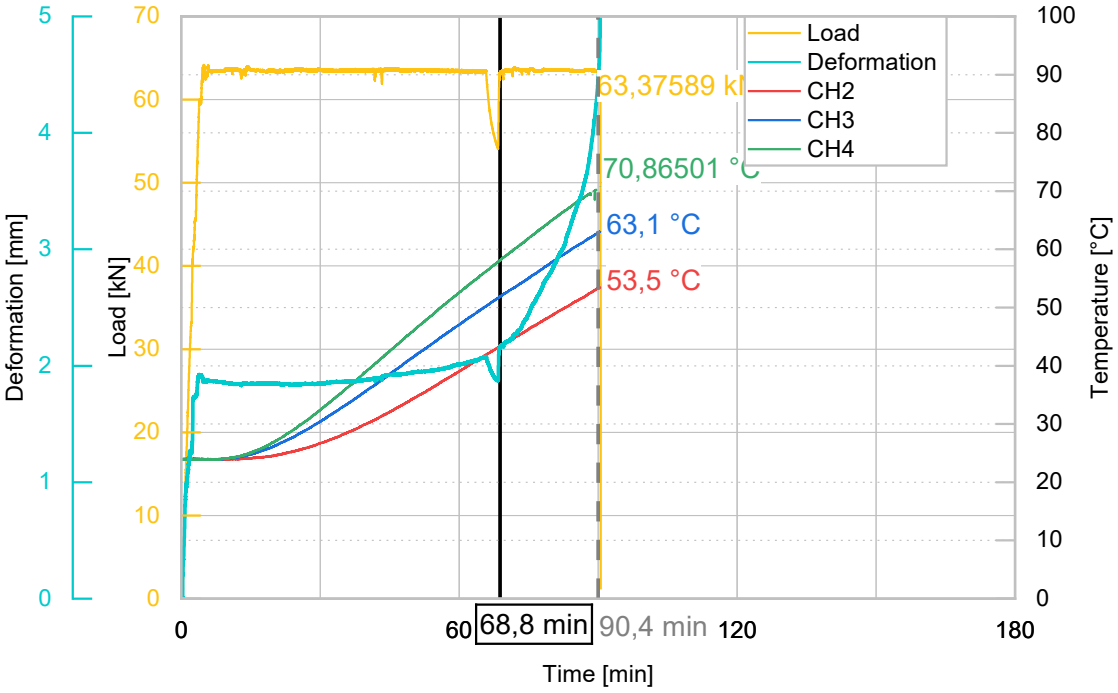

Figure 42: Load-deformation curve for specimen 31321

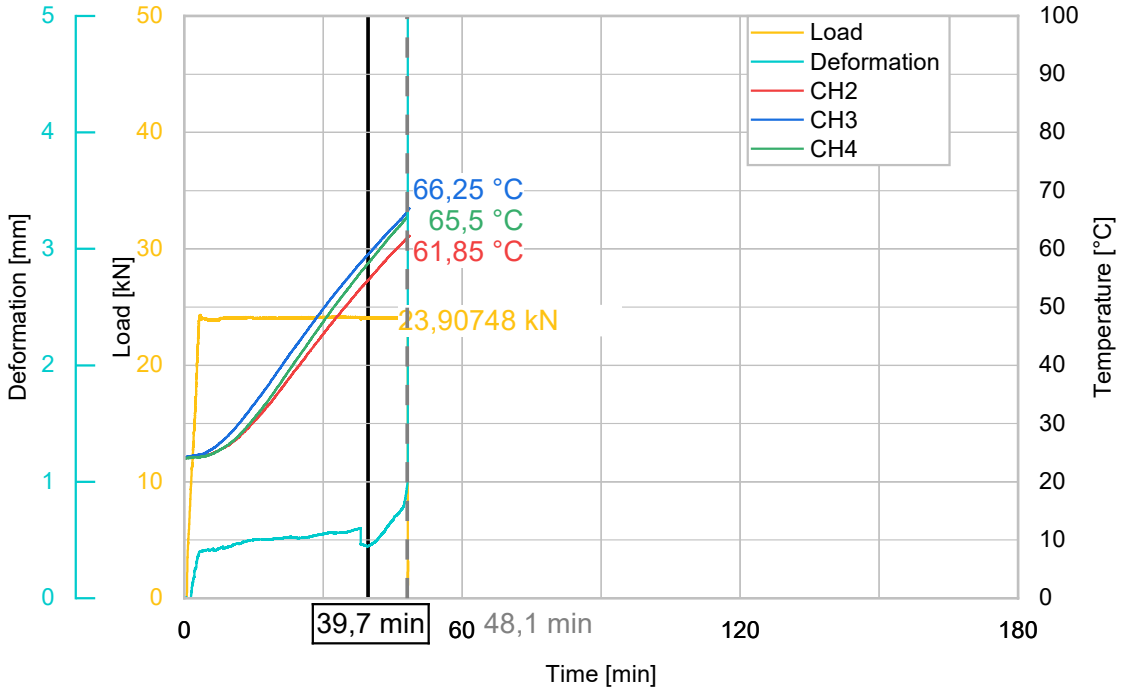

Figure 43: Load-deformation curve for specimen 32111

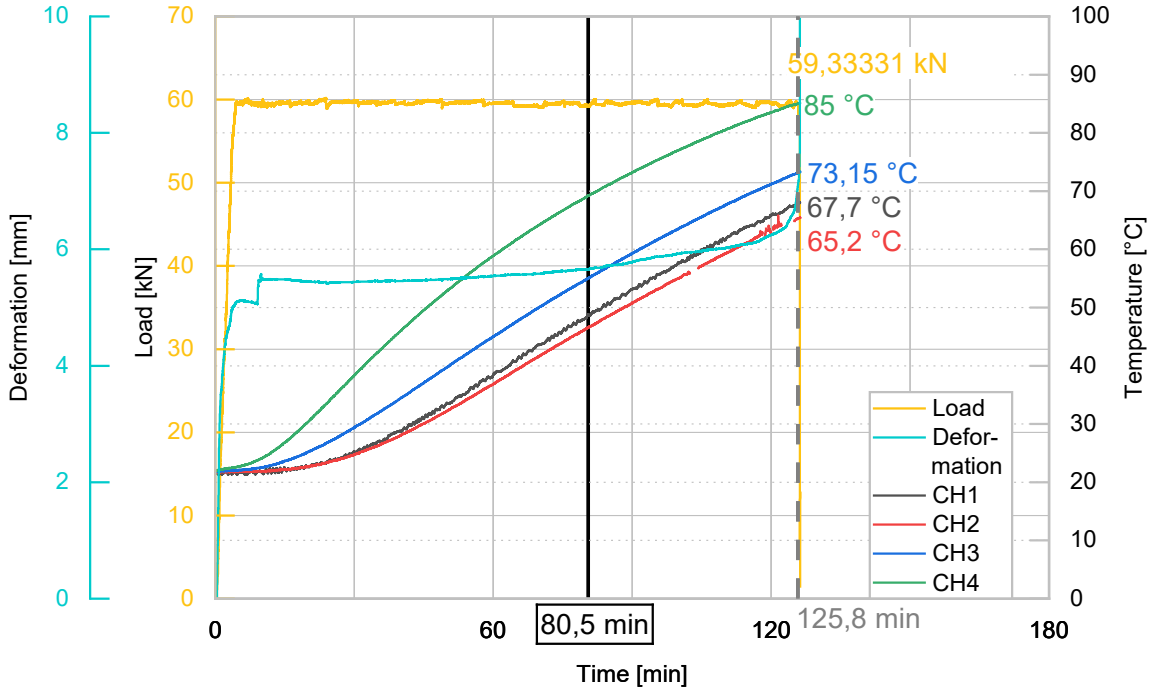

Figure 44: Load-deformation curve for specimen 32321

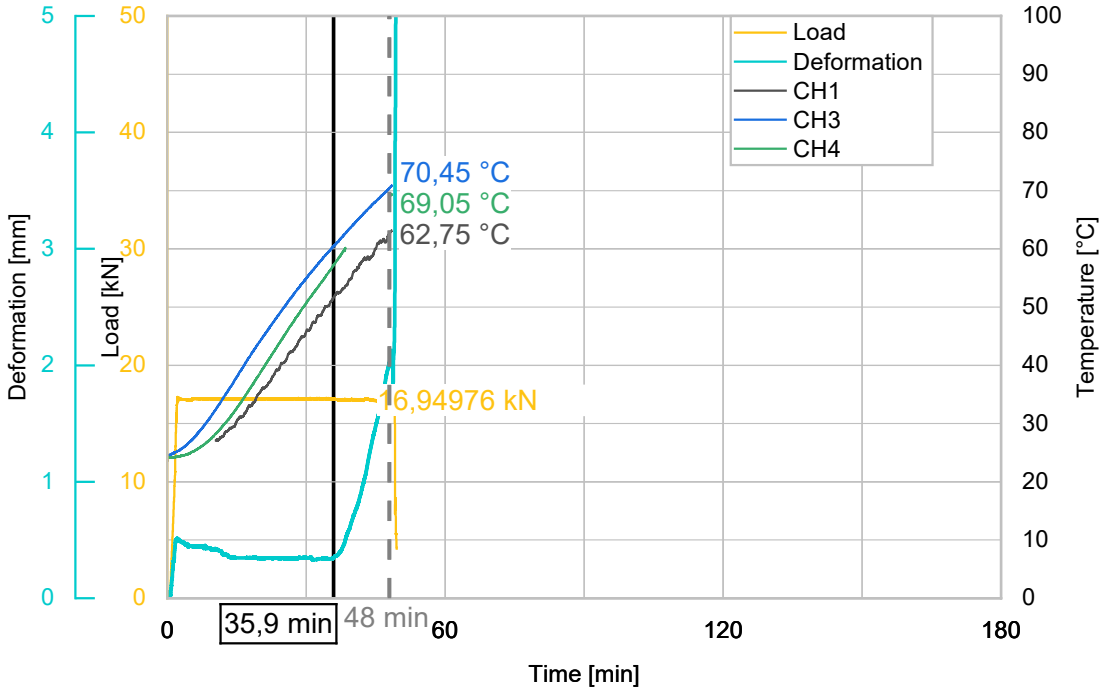

Figure 45: Load-deformation curve for specimen 41111

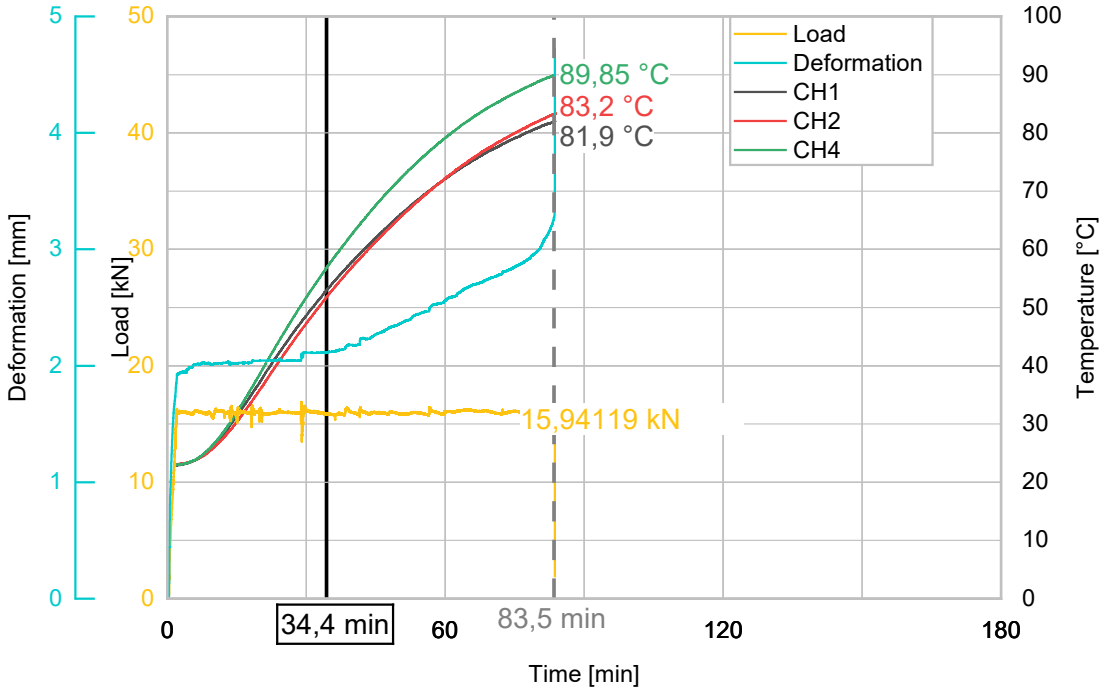

Figure 46: Load-deformation curve for specimen 42111

H Mean failure temperatures

Table 9: Failure temperatures for Adhesive 1 and Adhesive 2 (All: every specimen, 0,4 F: Specimens with 40 % reference load, 0,6 F: Specimens with 60 % reference load)

Adhesive 1

		All						60x60						100x100					
		All		0,4F		0,6F		All		0,4F		0,6F		All		0,4F		0,6F	
		T [°C]	σ	T [°C]	σ	T [°C]	σ	T [°C]	σ	T [°C]	σ	T [°C]	σ	T [°C]	σ	T [°C]	σ	T [°C]	σ
Adhesive failure only	Mean	70,78	0,09	71,88	0,09	63,10	0,00	64,78	0,06	64,78	0,06	-	-	72,78	0,09	74,72	0,07	63,10	0,00
	5%-Quantil	61,57		63,17		63,10		61,15		61,15		-		65,05		71,02		63,10	
	20%-Quantil	65,38		69,22		63,10		62,36		62,36		-		70,90		71,38		63,10	
All	Mean	69,92	0,08	71,48	0,08	65,22	0,03	67,05	0,05	67,44	0,06	66,28	0,03	72,78	0,09	74,72	0,07	63,10	0,00
	5%-Quantil	62,04		63,97		63,21		61,61		61,96		64,41		65,05		71,02		63,10	
	20%-Quantil	65,03		69,13		63,54		64,20		65,58		65,03		70,90		71,38		63,10	

Adhesive 2

		All						60x60						100x100					
		All		0,4F		0,6F		All		0,4F		0,6F		All		0,4F		0,6F	
		T [°C]	σ	T [°C]	σ	T [°C]	σ	T [°C]	σ	T [°C]	σ	T [°C]	σ	T [°C]	σ	T [°C]	σ	T [°C]	σ
Adhesive failure only	Mean	81,68	0,08	83,30	0,06	67,05	0,00	82,30	0,10	86,11	0,05	67,05	0,00	81,05	0,05	81,05	0,05	-	-
	5%-Quantil	69,91		75,88		67,05		69,56		80,49		67,05		74,77		74,77		-	
	20%-Quantil	78,36		79,99		67,05		77,09		83,14		67,05		78,88		78,88		-	
All	Mean	81,60	0,08	84,01	0,08	75,20	0,03	82,30	0,05	86,11	0,06	67,05	0,03	81,03	0,09	81,90	0,07	79,28	0,00
	5%-Quantil	70,23		79,83		67,69		69,56		80,49		67,05		75,11		80,35		73,99	
	20%-Quantil	79,60		80,51		69,59		77,09		83,14		67,05		80,25		80,64		75,75	